PIK Report

No. 101

AN ASYMPTOTIC, NONLINEAR MODEL FOR ANISOTROPIC, LARGE-SCALE FLOWS IN THE TROPICS

Stamen Dolaptchiev

POTSDAM INSTITUTE
FOR
CLIMATE IMPACT RESEARCH (PIK)

Diploma thesis submitted to the Department of Earth Science,
Free University Berlin, in February 2005

Author:
Dipl. Met. Stamen Dolaptchiev
Potsdam Institute for Climate Impact Research
P.O. Box 60 12 03, D-14412 Potsdam, Germany
Phone: +49-331-288-2621
Fax: +49-331-288-2620
E-mail: Stamen.Dolaptchiev@pik-potsdam.de

Herausgeber:
Prof. Dr. F.-W. Gerstengarbe

Technische Ausführung:
U. Werner

POTSDAM-INSTITUT
FÜR KLIMAFOLGENFORSCHUNG
Telegrafenberg
Postfach 60 12 03, 14412 Potsdam
GERMANY
Tel.: +49 (331) 288-2500
Fax: +49 (331) 288-2600
E-mail-Adresse:pik@pik-potsdam.de

ISSN 1436-0179 POTSDAM, SEPTEMBER 2005

Abstract

In order to investigate the atmospheric dynamics in the tropics, we applied an unified multiple scales asymptotic approach and derived reduced model equations. This technique combines methods from the multi-scale perturbation theory and the scale analysis in the theoretical meteorology. It can be used for multiple scales interaction studies. The systematic approach was applied to the 3D compressible equations for a fluid on an equatorial β-plane. An anisotropic asymptotic scaling was used, allowing to address flows on a sub-planetary length scale in zonal direction and on a mesoscale in meridional direction.

The reduced model equations consist of the WTG approximation and a nondivergent constraint on the flow in the y, z-plane. The momentum equation is time independent and have important nonlinear transport terms. The system of equations describes a model of a Hadley type circulation modified by a zonal pressure gradient force. After considering the magnitude of the different diabatic processes, we showed that convective heating will drive the circulation.

We have prescribed the potential temperature source term and analytical solutions for the meridional and vertical velocities were found. They describe ascending motions in the region of heating and descending in the region of cooling, a poleward flow in the upper and an equatorward flow in the lower atmosphere. To find solutions for the zonal wind, we considered the zonally averaged version of the x-component of the momentum equation. In the inviscid case we showed that the absolute zonal momentum per unit mass remains constant along stream lines. Numerical simulations were performed with a vertical diffusion representation of the turbulent momentum transport. The model predicts weak easterly surface winds and strong upper level westerlies at the boundary, corresponding to the subtropical jet at the edge of the Hadley cell. The meridional profile of the potential temperature is consistent with the geostrophic and hydrostatic balance in the model atmosphere. We have found that the momentum advection terms are large near the equator, especially in the region of heating.

Contents

Introduction

In the tropics there are phenomena, e.g. the El Niño Southern Oscillation (ENSO), the Madden-Julian oscillation or the monsoon circulation, which are characterized by different length and time scales. Variations in time are observed from minutes up to years and the spatial scales range from the micro scale up to the planetary scale. Another feature of the tropical circulation is the important coupling of the atmosphere and the ocean. Diabatic processes play here a crucial role and we have to mention that the complex interactions between convecting systems and the large-scale flow are not yet well understood. This is one of the reasons why an unique theory similar to the quasi-geostrophic theory is lacking for the tropics. But there are two major groups of simplified models, which represent our theoretical knowledge of the tropical atmosphere.

Simplified models capture the main processes in the atmosphere and are used to study interactions and to test sophisticated parameterizations. They have the advantage that the reduced model equations allow numerical solutions with very low computational costs or even analytical solution. Simplified models have relevant contribution to our understanding of the atmosphere. One group of such models for the tropics are the the Matsuno-Gill (Gill, 1980; Heckley and Gill, 1984) linear models of a steady circulation. They are driven by externally imposed diabatic heat source. The assumption is made that only the first baroclinic mode of the atmosphere is excited. The problem then can be reduced to solving the linear shallow water equations with a Rayleigh parameterization of the friction and the radiative cooling. Steady-state solutions are found under a long-wave approximation. They represent large-scale circulations like the Hadley and the Walker cells. Another class of simplified models are the recently developed weak temperature gradient (WTG) models (Sobel et al., 2001; Polvani and Sobel, 2002; Bretherton and Sobel, 2003). They are based on the assumption that the distribution of the temperature in the tropics is horizontally uniform. This agrees well with observations, e.g. there are no front systems in the tropics. It was shown that the basic features of the idealized Hadley and Walker circulation and of the Matsuno-Gill models are captured, when the WTG approximation is applied. The WTG method brings also simplifications when it is used in the quasi-equilibrium tropical circulation models for describing convectively coupled circulations (Bretherton and Sobel, 2002).

The foundation of the simplified models is a series of approximations. They are based on observations and are valid for certain regimes of the atmosphere only. The characteristic spatial and temporal scales of the regimes give the range of validity for the reduced model equations. The motivation for the neglect of particular terms in the governing equations cannot be easily accepted by people who are not familiar with the tropical meteorology. The scaling analysis is here a helpful tool to estimate the magnitude of the different forces. Klein (2000, 2004) proposed a multiple scales asymptotic approach for the derivation of reduced model equations. It combines the advantage of the scale analysis with methods from the perturbation theory. A

single non-dimensional parameter $\varepsilon \sim 1/8 \ldots 1/6$ is introduced and all characteristic numbers in the governing equations are expressed in terms of it. An asymptotic ansatz resolving the scales of interest is chosen. It is inserted in the governing equations and the terms, relevant for the considered regime, appear in the leading orders of the equations. Here we mention some important benefits of this approach:

- It is clear-cut and systematic method for deriving simplified models. It starts from the general $3D$ compressible flow equations and can be easily applied to different regimes.
- The derivation become more transparent, common mathematical arguments are used.
- Due to the fact that ε has a certain value, it is possible to calculate corrections to the leading order solutions and thus to obtain a better approximation to the "real" solution. The universal small parameter is an independent measure for the range of validity of the reduced model equations.
- The choice of the asymptotic ansatz allows us to study interactions between different scales. This is relevant especially for the tropics where phenomena with diverse temporal and spatial scales are coupled. Majda and Klein (2003) applied this technique and derived a model for the interactions between the synoptic and the planetary scale motions in the tropics.
- It is a starting point for the development of well-balanced numerical methods for different flow regimes.

Nevertheless additional physical considerations have to be always made, in order to find if the derived reduced model capture the important phenomena.

Motivated by the observed phenomena in the tropics and the theoretical achievements described above, we use this multiple scales asymptotic approach in order to derive reduced model equations. We applied the same scaling as for the seasonal sub-planetary equatorial WTG regime, derived in Majda and Klein (2003). The new equations represent a steady-state regime on a seasonal time scale. Its spatial scales of validity are anisotropic – a sub-planetary length scale in zonal direction and a mesoscale in meridional direction. The regime contains the 3D generalization of the WTG approximation, it describes a zonally symmetric circulation, driven by convective heating, and embedded in a zonal pressure gradient field. The zonally averaged version of the equations is an idealized model of a Hadley cell (Schneider and Lindzen, 1977; Schneider, 1977; Held and Hou, 1980; Fang and Kit Tung, 1999). Analytical and numerical solutions are found for this case.

The outline of this study is as follows: the main atmospheric phenomena in the tropics are reviewed in Chapter 1. They give the physical motivation for the scaling used in the asymptotic expansion. The Hadley cell and its role for the transport of momentum is also discussed. In Chapter 2 we introduce the multiple scale asymptotic approach, the reduced model equations are derived. In Chapter 3 we consider the unresolved processes which are important for the dynamics. A parameterization is chosen for the turbulent transport of momentum and for the convection, which has the main contribution to the diabatic source term. Analytical solutions for the vertical and meridional velocities and for the vertically integrated potential temperature

are found and discussed in Chapter 4. Solutions for the zonal wind in the inviscid case and with a simple representation of the friction are given. Chapter 5 is devoted to numerical solutions using a more realistic parameterization of the momentum sink. The numerical method and simulations with different model setups are presented. At the end there is a brief summary of the results.

Chapter 1

Tropical circulation

In this chapter a brief review of the main atmospheric phenomena in the tropics is given. The issue of the interactions between the convection and the large-scale flow is addressed. We concentrate on the Hadley cell as an idealized model of a tropical circulation, its role in the momentum budget is elucidated.

1.1 Observations of the tropical circulation

One commonly used model of the tropical circulation is the thermally driven Hadley cell – warm air raising near the equator, flowing poleward in the upper troposphere, descending in the subtropical regions and moving in the lower atmosphere back to the equator. Thus the inflow of air at the equator forms the intertropical convergence zone (ITCZ), see Fig. 1.1. It can be easily recognized on a satellite image of the earth as a narrow band of cumulus clouds. But after precise view, we will observe that this belt is almost never at the equator and it is not continuous. It is made rather by a number of deep convective cloud systems. These clusters play a central role in the energy balance of the atmosphere. Individual cumulonimbus reach the top of the troposphere at $\approx 16\,\mathrm{km}$, they are sometimes referred to as undiluted hot towers. With vertical velocities of the order of $1\,\mathrm{m\,s^{-1}}$ in the cores, they pump moist air from beneath the trade inversion in the upper atmosphere. The air parcels inside the clouds undergo a pseudoadiabatic ascent, nearly without entrainment of dry air from the environment and they release a significant amount of latent heat.

Satellite images show that the temporal and spatial distribution of the cloudiness over the tropics varies and the precipitation is not confined in the ITCZ. Westward propagating equatorial wave disturbances are the reason for such phenomena. They have a period of $\approx 5\,\mathrm{days}$, a length of $3000-4000\,\mathrm{km}$ and a propagation speed of $8-10\,\mathrm{m\,s^{-1}}$. The troughs of these waves coexist with the area of deep cumulus convection. The released latent heat there causes vertical flows and thus drives the secondary circulation needed to sustain the wave.

Another important feature of the tropics are the Walker-type circulations resulting from east-west SST gradients. In some regions (tropical Pacific) such cells dominate over the Hadley circulation. They have length scales of $\sim 15000\,\mathrm{km}$ and are connected with an intensive convection (western Pacific) (Peixoto and Oort, 1992).

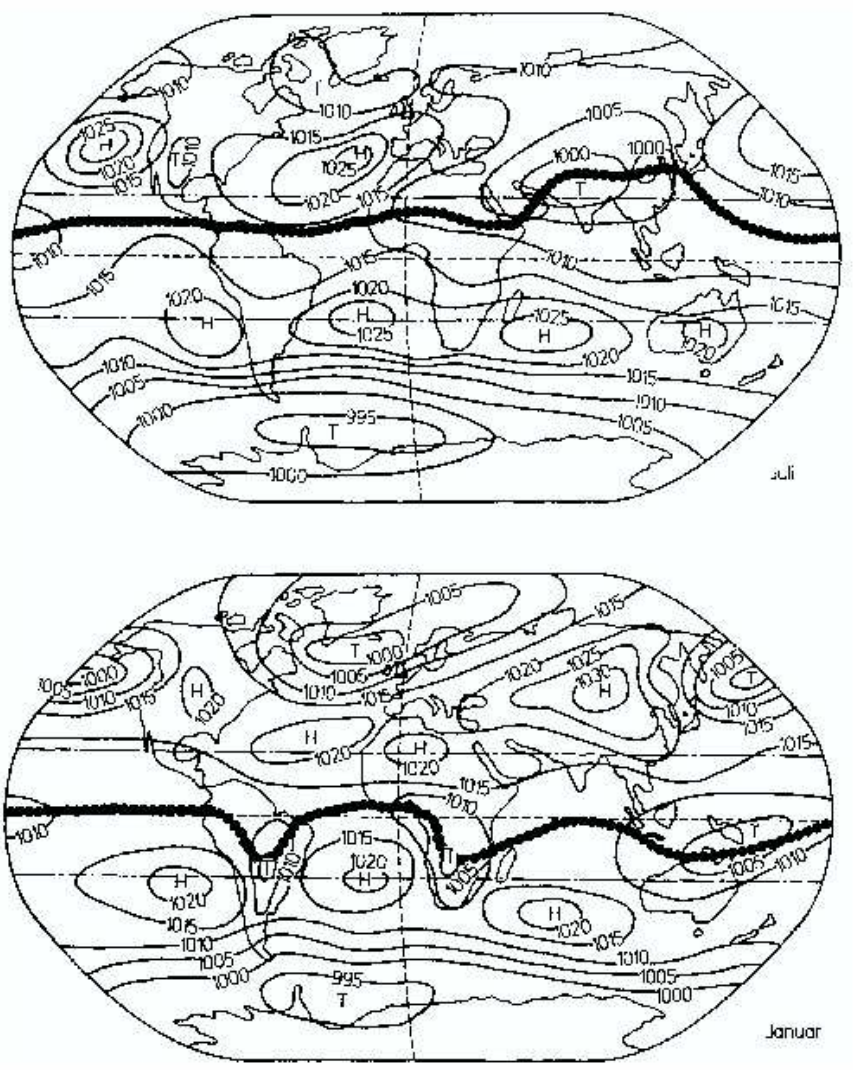

Figure 1.1: The position of the ITCZ for July (upper plot) and January (lower plot) (Roedel, 1994)

The observed SST anomalies and the resulting sea pressure gradients, associated with the Walker circulation, have fluctuations on different time scales. They are explained as an internal oscillation of the atmosphere-ocean system. The strongest such signal is the El Niño Southern Oscillation – ENSO. It has a period of $2-5$ years and is associated with surface drag anomalies of the trade winds in the Pacific, they excite Kelvin and Rossby waves in the ocean. The waves produce the upwelling of the thermocline and SST changes, pressure anomalies result (Peixoto and Oort, 1992).

Madden and Julian (1971) discovered an additional high frequency oscillation in the tropics. It has a period of $30-60$ days and is often referred to as the intraseasonal oscillation. It is connected with the eastward movement of a large-scale cell in the atmosphere. The triggering mechanism has not yet been understood - an extratropical forcing or penetrating Rossby waves from the mid-latitudes are possible explanations.

Finally, circulations on a seasonal time scale are observed in the tropics, driven by the temperature contrast over the land and the ocean (e.g. the Indian monsoon). The deep convection plays here a crucial role in magnifying the strength of the overturning and spreading it over the whole depth of the atmosphere. In a non-convecting atmosphere such circulation is confined only to the boundary layer.

It is important to note the anisotropy of many phenomena in the tropics (e.g. Madden-Julian Oscillation, ENSO, Walker cell), their zonal length scale is an order of magnitude larger than the meridional scale. Fields of surface pressure or SST have also such anisotropic distribution. In the tropics we have the equatorial wave guide (Gill, 2003), waves are confined in the equatorial belt and can propagate primarily in zonal direction.

1.2 Convection and the large-scale flow

The theory of the interactions between convective cloud systems and the large-scale circulation has been characterized by some significant changes during the last years.

Charney and Eliassen (1964) introduced the concept of convective instability of the second kind (CISK) as an explanation for the development of hurricanes. It is based on the idea that a large-scale cyclonic disturbance supplies moisture for the convecting region embedded in it through boundary layer convergence (Ekman pumping). The convective system on the other hand intensifies the secondary circulation (ascending air in the cyclonic disturbance) and thus has a positive feedback on the large-scale motion. This view of convection has dominated for some years in the atmospheric science community and convective parameterizations based on CISK assumptions has been developed (Kuo, 1974). These convective schemes were derived using moisture budgets, assuming that the difference between surface evaporation and precipitation is nearly balanced by moisture convergence. Emanuel et al. (1994) emphasized that this convective parameterization fails to reproduce realistic radiative-convective equilibrium without a large-scale disturbance. This class of schemes concentrates on the determination of the heating (release of latent heat) without considering the complicated interactions between the cloud system and the environment. This is an ”external” view of cumulus heating, because an imposed external heat source will produce positive temperature fluctuations, but this is not always true in the case of convecting atmosphere.

New ideas on convection were presented in the paper of Arakawa and Schubert (1974), where they introduced the quasi-equilibrium parameterization. They make the assumption that the time scales of response of the convecting system $\sim$ 1 h are much less then those describing the large-scale system. This means that the available potential energy (APE) produced by the large-scale motion is almost fully converted into kinetic energy by the convection (vertical motions) and after that dissipates (turbulence). So there is no accumulation of APE, which can result in increasing the kinetic energy of the large-scale circulation. This statement rejects the fundamental hypothesis in CISK. In the new theory, the convective atmosphere tends to remove conditional instability of the first kind (Arakawa and Schubert, 1974). Emanuel et al. (1994) introduced the statistical-equilibrium thinking. They connect the virtual temperature in a convecting atmosphere with the sub-cloud layer entropy (represented by the pseudoadiabatic potential temperature θ_e). The sub-cloud layer entropy is influenced by sensible, latent and

radiative heat fluxes, fluxes of low entropy air from the middle troposphere (downdraughts), entraining air from the cloud free area of the lower atmosphere. It was shown that large-scale ascent will result in reduction of the sub-cloud layer entropy (through downdraughts of the intensified convection) and thus produce a cooling in the free-atmosphere – a positive effective static stability. An effective stability is the static stability of the atmosphere, where the effect of condensation is included implicitly.

Another important feature of the quasi-equilibrium approach is the consideration of the interactions between ocean and atmosphere. Here we mention two important examples. The first is the influence of the sea surface temperatures (SST) on the subcloud layer entropy and thus on convection. The coincidence of the position of the ITCZ and the regions with the highest SST proves such strong connection. The second is the evaporation-wind feedback. Stronger surface winds increase the evaporation from the oceans and the gained moisture will amplify the convection. So intensified downdraughts and winds will occur. Observations of hurricanes indicate such mechanism.

The main idea that the atmosphere tends to remove convective instability of the first kind was implemented in different convective schemes (Arakawa and Schubert, 1974; Betts, 1986; Betts and Miller, 1986).

Recently some quasi-equilibrium tropical circulation models (QTCMs) have been developed (Neelin and Zeng, 2000; Zeng et al., 2000; Bretherton and Sobel, 2002) in order to investigate the influence of such convective parameterization on the atmospheric circulation.

1.3 The Hadley cell

Hadley (1735) proposed the idea of thermally direct circulation with ascending warm air at the equator, flowing poleward in the upper atmosphere and with cold air moving equatorward in the lower troposphere, see Fig. 1.2.

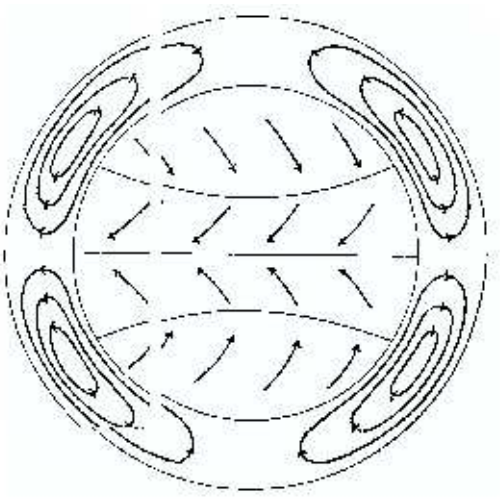

Figure 1.2: The general circulation of the atmosphere, by Hadley (1735)

With this model he could explain the trade winds but not the observed westerlies in the midlatitudes (Hadley supposed that the circulation will spread from the equator to the poles).

Farrel (1856) and Thomson (1857) introduced an additional thermally indirect cell and this modified model could elucidate the surface winds. The transport of angular momentum in the atmosphere was investigated 1926 by Jeffreys. In his study he neglected the contribution to the Hadley cell referring the main part to eddies and for some time the role of the Hadley circulation was underestimated.

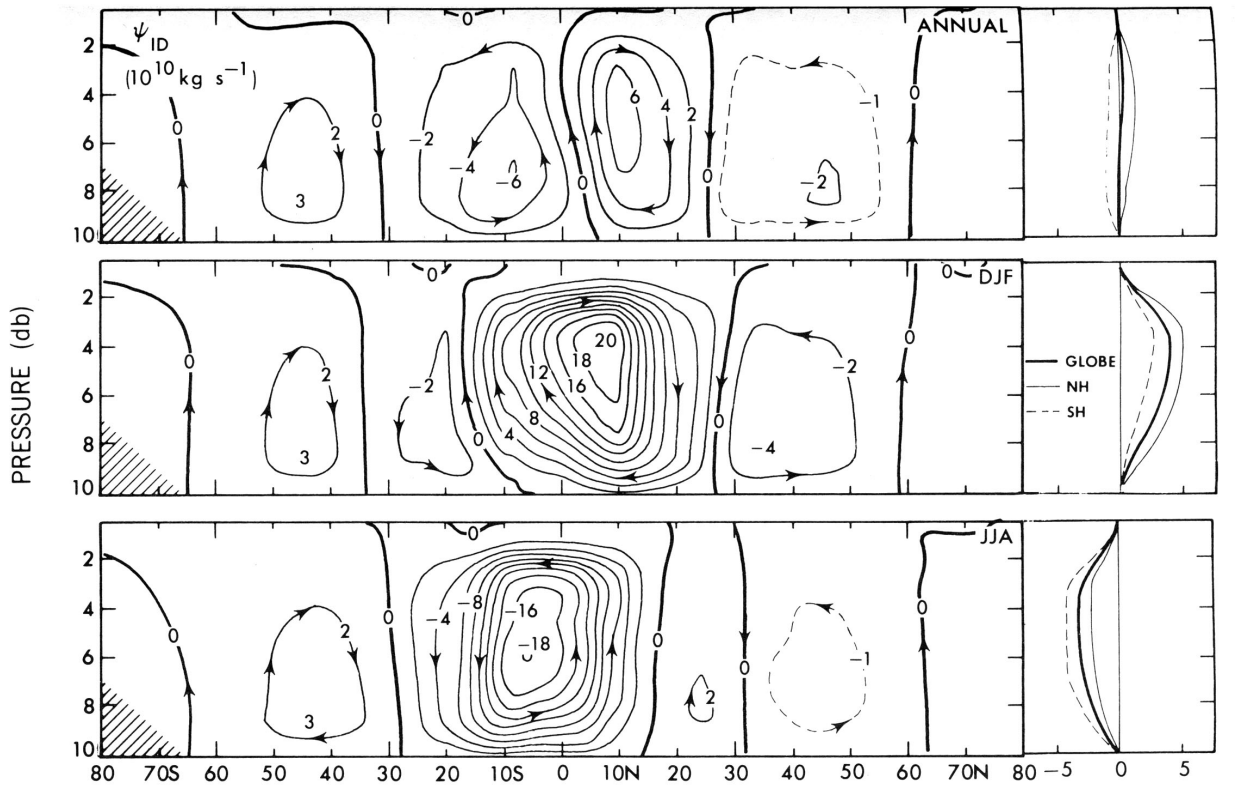

Figure 1.3: The observed mass stream function ψ for the zonally averaged circulation (Peixoto and Oort, 1992)

First Schneider and Lindzen (1977) tried to answer the question to what extent thermally direct cells are responsible for the observed general circulation. Taking the 3D compressible flow equations on a rotating sphere, they have performed some numerical simulations of zonally symmetric steady circulation, excluding the effect of eddies (barotropic, baroclinic and topographic eddies). Their results can be interpreted as a consistent basic state of the circulation, which can be used for instability studies. Schneider and Lindzen (1977) showed that a circulation driven by the radiative-equilibrium temperature difference between the equator and the pole, will be very weak and confined primarily in the boundary layer. Only with the inclusion of an upper level heating, due to deep cumulus convection (latent heat release), and cumulus friction (vertical transport of horizontal momentum in the cumulus clouds), they were able to simulate a meridional circulation close to the magnitude of the observed. Experiments were performed with different distributions of the convective heating: resembling the narrow heating due to the ITCZ, or such derived from annual mean precipitation rates. In his nonlinear model

Schneider (1977) included a crude parameterization of the release of latent heat, linking it to the evaporation and the moisture convergence (below the trade inversion). In their simulations Schneider and Lindzen (1977) reproduced the zonally averaged mean circulation in the tropics and the observed subtropical jet in the upper troposphere.

Held and Hou (1980) presented a detailed discussion of the Hadley cell for a Boussinesq fluid on a rotating sphere, driven by meridional temperature differences. For the nearly inviscid case they gave some analytical solutions for the zonal wind at the top of the atmosphere, the surface winds, the meridional temperature transport and the vertically integrated distribution of the potential temperature. Numerical experiments for a viscous fluid were also performed and were in good agreement with the analytical solutions.

It is important to mention that only the annual mean general circulation shows a structure with two symmetric Hadley cells. Observations indicate that we have over the most period of the year a strong winter cell and a weak summer cell (see Fig. 1.3 middle and lower plot). This fact motivated Lindzen and Hou (1988) to investigate the asymmetry of the heating about the equator. They simulated the intensification of the winter Hadley cell and the winter easterlies, due to the increased meridional temperature gradients in the winter hemisphere.

Recent studies were devoted to the time-dependent Hadley circulation (Fang and Kit Tung, 1999). They show that the simulated strength of the cell is close to the observed, when the annual variations of the heating are included.

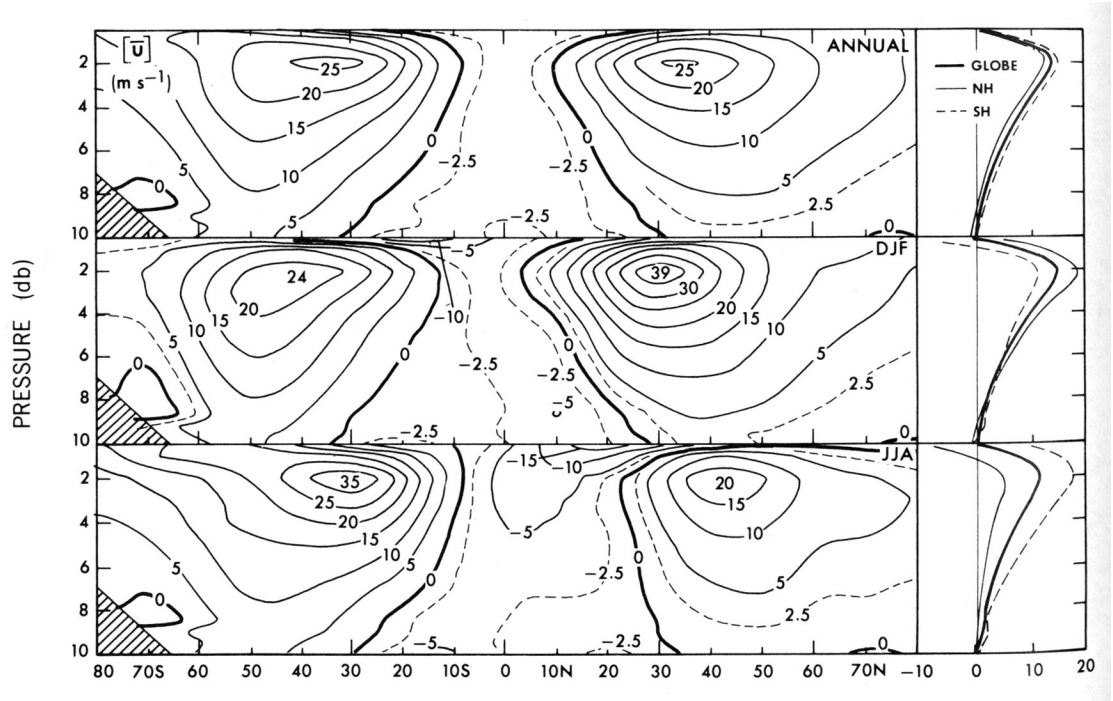

Figure 1.4: The observed zonal winds (Peixoto and Oort, 1992)

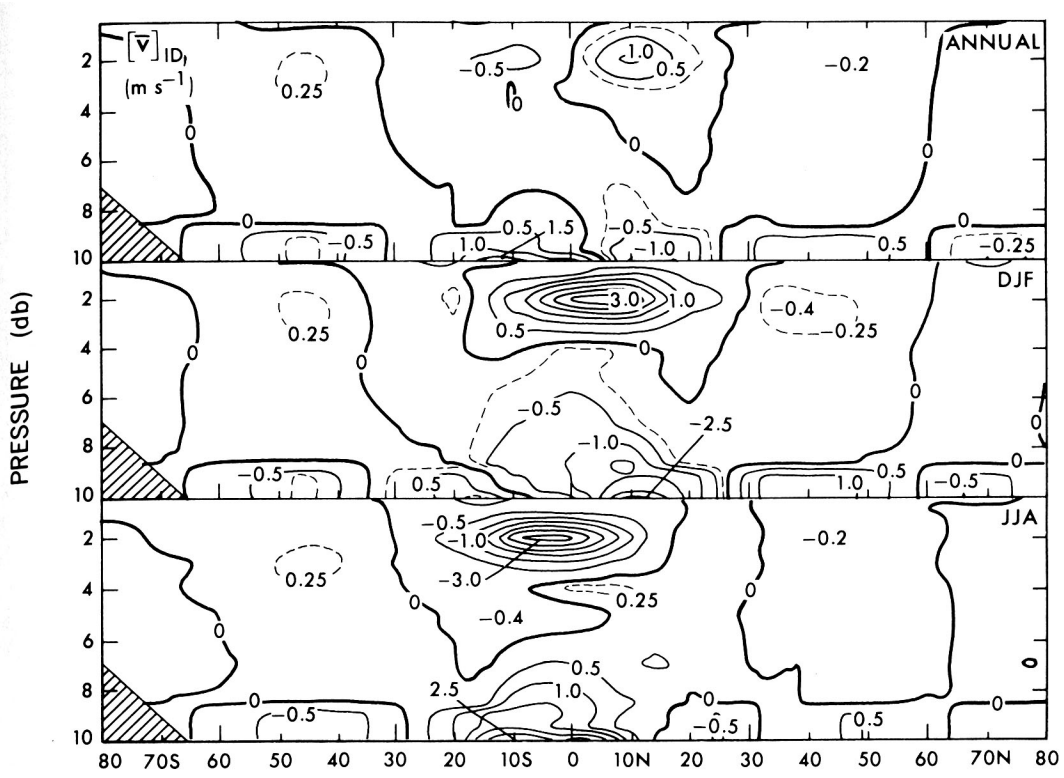

Figure 1.5: The observed meridional winds (Peixoto and Oort, 1992)

1.4 Meridional transport of momentum

The Hadley cell plays an important role not only in the energy balance of the atmosphere (pumping warm air poleward and cold air equatorward and thus reducing the meridional temperature gradient), but also in the angular momentum budget. The absolute angular momentum M is defined as $M = \Omega a^2 \cos^2 \phi + ua \cos \phi$, where Ω and a are the rotation frequency and the radius of the earth, ϕ denotes the latitude and u is the zonal velocity. This relationship is similar to the definition of the total momentum p_x on a β plane (see (4.40)). In the tropics the observed surface winds are easterlies and in the higher latitudes westerlies. This means that in the tropics the absolute angular momentum of the atmosphere is less then that of the rotating earth and in the midlatitudes is the opposite. Through surface drag the earth continuously looses angular momentum to the atmosphere in the tropics and gains in the higher latitudes. Since our planet rotates with nearly constant frequency the total angular momentum of the earth remains constant, so these two processes must compensate. There has to be a net flux of angular momentum in the atmosphere from the tropics to the poles. This transport is realized through eddies and symmetric circulations. The Hadley cell has an important contribution to it. The ascending air in the equatorial region has the highest values of angular momentum and it is transported poleward. The earth's angular momentum decreases toward the pole, and thus a surplus of momentum in the atmosphere at higher latitudes is created. This is the reason for the existence of the subtropical jet (see Fig. 1.4), who changes its position and strength during the year in accordance with the Hadley circulation. Because of the hydrostatic balance of the atmosphere, the strong upper level zonal winds require a meridional temperature gradient (see Fig. 1.6). The

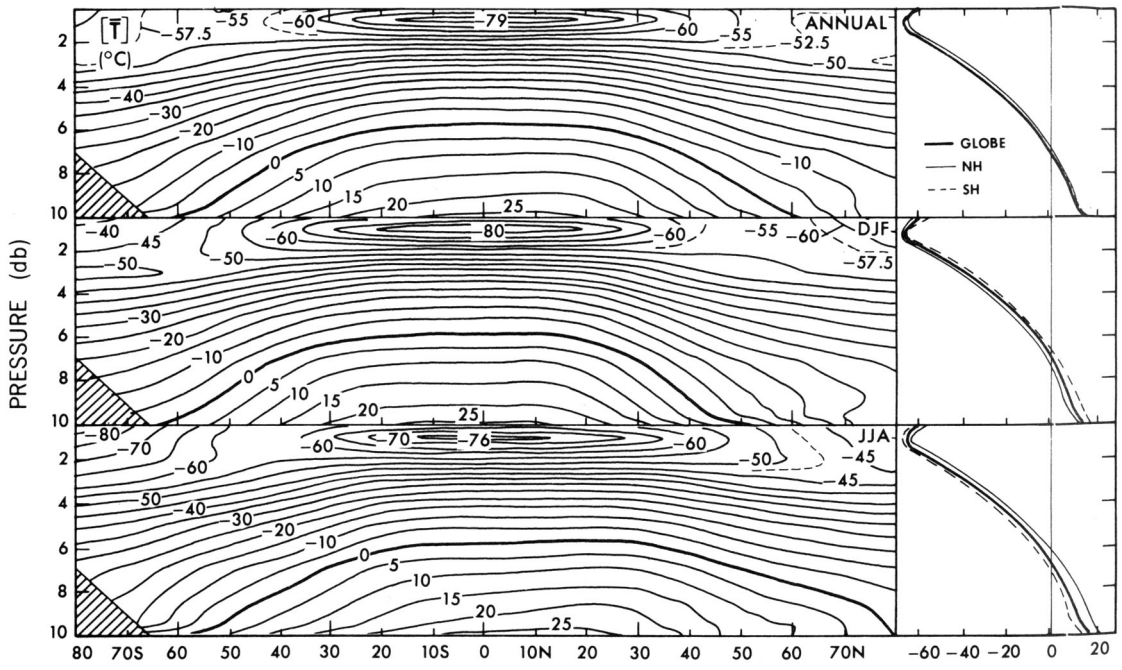

Figure 1.6: The observed zonally averaged temperature (Peixoto and Oort, 1992)

surplus of relative momentum of the air is transferred back to the surface by friction (see the zonally mean winds near the surface in Fig. 1.4 and 1.5).

In order to investigate the meridional transport of momentum [1] , we multiply the x-component of the momentum balance equation (2.59) with ρ and integrate over z

$$\int_0^1 \rho v \partial_y u \, \mathrm{d}z + \int_0^1 \rho w \partial_z u \, \mathrm{d}z - \int_0^1 \beta \rho y v \, \mathrm{d}z = \int_0^1 \partial_z \mu \partial_z u \, \mathrm{d}z \,, \tag{1.1}$$

where at $z = 1$ is the top of the atmosphere. For the representation of the source term S_u see Chapter 3. The contribution of the third term on the l.h.s of (1.1), describing the transport of earth's momentum by the meridional mass flux is zero, because there is no net surplus or deficit of mass in a vertical column air (we are interested in steady circulations). This can be easily seen if we introduce a mass stream function ψ(for the definition see (4.1),(4.2)). The third integral on the l.h.s of (1.1) can be rewritten as

$$\beta y \int_0^1 \partial_z \psi \, \mathrm{d}z = \beta y \big(\psi(z=1) - \psi(z=0) \big) = 0 \,, \tag{1.2}$$

where we have used $\psi = const$ at the boundary of the circulation which implies no mass transport out of the considered domain. For the r.h.s. of (1.1) we use a stress free boundary

[1] In Chapter 2 we derive reduced model equations (2.59)-(2.62). For consistency we will address the meridional transport of momentum using this system of equations. The same discussion can also be applied to the zonally averaged steady-state governing equations for geostrophically balanced flow, leading to the same results.

condition at the top for $z = 1$ and the usual bulk formula for the representation of the surface shear

$$\int_0^1 \partial_z \mu \partial_z u \, \mathrm{d}z = \mu \partial_z u \Big|_{z=1} - \mu \partial_z u \Big|_{z=0} = -Cu^2(z=0)\,. \tag{1.3}$$

Finally, the vertically integrated equation for the zonal momentum takes the form

$$\int_0^1 \rho v \partial_y u \, \mathrm{d}z + \int_0^1 \rho w \partial_z u \, \mathrm{d}z = -Cu^2(z=0)\,. \tag{1.4}$$

This equation states that the flux of relative momentum is balanced by the surface drag. An important conclusion is that in a linear model the surface winds must be set to zero, if the parameterization of the friction term, leading to the r.h.s. in (1.4) is used.

Chapter 2

Multiple Scales Asymptotic Approach

The multiple scales asymptotic approach has several key points, discussed briefly below and applied to the governing equations for a 3D compressible flow on a β-plane. The scaling we use is motivated by the phenomena described in Chapter 1. New reduced model equations are derived, they characterize flows on a meso and sub-planetary length scales and a seasonal time scale.

In order to investigate the dynamics in the tropics, an unified mathematical modeling approach has been used, proposed by Klein (2000, 2004). The technique is based on multi-scale perturbation theory. It makes the scale analysis in the theoretical meteorology transparent and can be used for multiple scales interactions studies. Klein (2000, 2004) derived some well-known quasi-geostrophic atmospheric regimes, using this unified mathematical approach. Majda and Klein (2003) applied it and deduced a hierarchy of multi-scale reduced equations describing scale interactions in the tropics.

The multiple scale asymptotic approach consists of the following steps:

1. Non-dimensionalize the governing equations using some physical reference quantities with well defined values and independent of the considered length and time scales.

2. These reference quantities form some well-known non-dimensional numbers such as the Rossby, Froude and Mach numbers. A small parameter ε is introduced and the characteristic numbers are expressed in terms of it in a distinguished limit.

3. To be able to consider the length and time scales of interest, we choose special asymptotic expansion. The derivation of the reduced equations is then straightforward: the ansatz is substituted in the governing equations and the terms of the same order are equated.

2.1 Dimensionless governing equations

We choose some physical parameters, that do not change significantly in different atmospheric flow regimes. Definitely, such quantities for the earth and for the atmosphere are:

rotation frequency:	$\Omega \sim 7\ 10^{-5}\,\mathrm{s}^{-1}$
radius:	$a \sim 6\ 10^{3}\,\mathrm{km}$
gravity acceleration:	$g \sim 10\,\mathrm{m\,s}^{-2}$

Table 2.1: Reference quantities for the earth

scale height:	$h_{sc} \sim 10^{4}\,\mathrm{m}$
thermodynamic pressure:	$p \sim 10^{5}\,\mathrm{kg\,m}^{-1}\,\mathrm{s}^{-2}$
air density:	$\rho \sim 1\,\mathrm{kg\,m}^{-3}$
air velocity in the tropics:	$v \sim 5\,\mathrm{m\,s}^{-1}$

Table 2.2: Reference quantities for the atmosphere

Using these reference quantities the dimensionless governing equations for a compressible flow take the form:

$$\partial_t \boldsymbol{u} + \boldsymbol{u}\cdot\nabla\boldsymbol{u} + w\boldsymbol{u}_z + \frac{1}{Ro}(\boldsymbol{f}\times\boldsymbol{v})_{\parallel} + \frac{1}{M^2}\frac{1}{\rho}\nabla p = \boldsymbol{S_u} \tag{2.1}$$

$$\partial_t w + \boldsymbol{u}\cdot\nabla w + ww_z + \frac{1}{Ro}(\boldsymbol{f}\times\boldsymbol{v})_{\perp} + \frac{1}{M^2}\frac{1}{\rho}p_z + \frac{1}{Fr^2} = S_w \tag{2.2}$$

$$p_t + \boldsymbol{u}\cdot\nabla p + wp_z + \gamma(\nabla\boldsymbol{u} + w_z) = \rho S_p \tag{2.3}$$

$$\theta_t + \boldsymbol{u}\cdot\nabla\theta + w\theta_z = S_\theta \tag{2.4}$$

$$\rho = \frac{p^{\frac{1}{\gamma}}}{\theta} \tag{2.5}$$

Where $\boldsymbol{f}$ is the earth rotation unit vector, γ is the isentropen exponent, $M,\ Fr$ and Ro are the Mach, Froude and Rossby numbers, $\boldsymbol{S_u}$, $S_w,\ S_p,\ S_\theta$ denote source terms, $\boldsymbol{v}, \boldsymbol{u}, w, \rho, \theta$ are the non-dimensional velocity vector, horizontal velocity vector, vertical velocity, density and potential temperature, respectively.

2.2 The distinguished limit

The non-dimensional numbers are defined as:

$$M = \frac{v_{ref}}{\sqrt{p_{ref}/\rho_{ref}}} \sim \mathcal{O}(\tfrac{1}{30})\,, \tag{2.6}$$

$$Fr = \frac{v_{ref}}{\sqrt{gh_{sc}}} \sim \mathcal{O}(\tfrac{1}{30})\,, \tag{2.7}$$

$$Ro = \frac{v_{ref}}{2\Omega h_{sc}} \sim \mathcal{O}(8)\,. \tag{2.8}$$

Here we give some typical values for the characteristic numbers, inserting our reference quantities in the definitions. Notice that the Rossby number is "large", because we have used h_{sc} as a reference length. If we use a typical synoptic scale $\sim 1000\,\text{km}$, it would be also small. In the asymptotic, the small numbers (like M and Fr) and the large (Ro) are expressed in terms of small parameters. If we use for each number a different small parameter, it would lead to complications and not unique solutions. Suppose we have two small parameters ε and δ, then our result will depend on the way we take the limit: e.g. if we first let $\varepsilon \to 0$ and then $\delta \to 0$, the reverse order or we use some coupling between the two parameters. Klein (2000, 2004) showed that, choosing a particular dependence on one and the same ϵ for all non-dimensional numbers, it is possible to derive some well-known model equations in the meteorology. Following Klein (2000, 2004) we introduce the same distinguished limit:

$$M = \varepsilon^2 \widehat{M}\,, \tag{2.9}$$

$$Fr = \varepsilon^2 \widehat{Fr}\,, \tag{2.10}$$

$$Ro = \frac{1}{\varepsilon}\widehat{R_o}\,, \tag{2.11}$$

where $\widehat{M},\ \widehat{Fr},\ \widehat{Ro} = \mathcal{O}(1)$, as $\varepsilon \to 0$ and will be set to unity hereafter. Taking into account the magnitude of $M,\ Fr,\ Ro$ see (2.6),(2.7) and (2.8), we can estimate $\varepsilon = \frac{1}{8} \ldots \frac{1}{6}$, which is sufficient to use ε as a small parameter for the asymptotic expansion later.

2.3 The Coriolis term and the equatorial β-plane approximation

We consider dynamics confined in the tropics and apply the β-plane approximation to the governing equations. For a latitude φ_0 the perpendicular projection of the earth rotation unit vector is given by

$$\begin{aligned} |\boldsymbol{f}_\perp| = \sin(\varphi_0 + \frac{y'}{a}) = \sin(\varphi_0 + \underbrace{\frac{y'}{h_{sc}}}_{y}\underbrace{\frac{h_{sc}}{a}}_{\varepsilon^3}) = \\ = \sin(\varphi_0) + \varepsilon^3 y \cos(\varphi_0) + \mathcal{O}(\varepsilon^6) \end{aligned} \tag{2.12}$$

Here a represents the earth radius $\approx 6000\,\text{km}$, y' denotes the distance from the equator and y is the same in non-dimensional form. At the equator $\varphi_0 = 0$ and the Coriolis term can be written in terms of ε as:

$$\frac{1}{R_o}(\boldsymbol{f} \times \boldsymbol{v})_\parallel = \varepsilon^4 y \boldsymbol{k} \times \boldsymbol{u} + \varepsilon \boldsymbol{j} \times \boldsymbol{k} w + \mathcal{O}(\varepsilon^7). \tag{2.13}$$

Under the β-plane approximation the governing equations take the form

$$\partial_t \boldsymbol{u} + \boldsymbol{u} \cdot \nabla \boldsymbol{u} + w \boldsymbol{u}_z + \varepsilon^4 y \boldsymbol{k} \times \boldsymbol{u} + \varepsilon w \boldsymbol{i} + \varepsilon^{-4} \frac{1}{\rho} \nabla p = \boldsymbol{S_u}\,, \tag{2.14}$$

$$\partial_t w + \boldsymbol{u} \cdot \nabla w + w w_z + \varepsilon (\boldsymbol{f} \times \boldsymbol{v})_\perp + \varepsilon^{-4} \frac{1}{\rho} p_z + \varepsilon^{-4} = S_w\,, \tag{2.15}$$

$$p_t + \boldsymbol{u} \cdot \nabla p + w p_z + \gamma (\nabla \boldsymbol{u} + w_z) = \rho S_p\,, \tag{2.16}$$

$$\theta_t + \boldsymbol{u} \cdot \nabla \theta + w \theta_z = S_\theta\,. \tag{2.17}$$

2.4 Expansion scheme

In addition to our reference quantities we introduce some other length and time scales, which are suitable for addressing large-scale flows in the tropics.

The main atmospheric phenomena in the tropics are described briefly in Chapter 1. They motivate our interest on dynamics on a seasonal time scale with a length scales in the range of $500 - 2000\,\text{km}$. The Charney inertial radius is intuitively a characteristic length scale of such flows:

$$l_m = \sqrt{\frac{v_{ref}}{\beta}} \sim 500\,\text{km}\,. \tag{2.18}$$

It gives the length scale on which rotational effects begin to affect an inertial atmospheric flow. The corresponding advective time is given by:

$$t_m = \frac{l_m}{v_{ref}} \sim 1.1\,\text{days}\,. \tag{2.19}$$

L_m and t_m will be called hereafter mesoscale length and time scale, using the terminology of Majda and Klein (2003). In the tropics there are often interactions with larger scale disturbances, which typically propagate in the zonal direction (in meridional direction the flow is confined, we have the equatorial wave guide as shown by Gill (2003)) and have a length scale $2000 - 14000\,\text{km}$. So we introduce a sub-planetary length scale

$$L_{sP} = \varepsilon^{-1} l_m \sim 5000\,\text{km}\,,$$

with an advection time scale:

$$T_s = \varepsilon^{-1} t_m \sim 11\,\text{days}$$

referred to as seasonal time scale.

Coordinates scaling

The next step is to express the coordinates, resolving the spatial and temporal scales of interest. First the length scales are written in terms of the scale height

$$l_m = \varepsilon^{-2} h_{sc}\,, \tag{2.20}$$
$$L_{sP} = \varepsilon^{-3} h_{sc}\,. \tag{2.21}$$

Suitable coordinates are obtained if we non-dimensionalize them by $l_m,\ L_{sP}$. Because the variables of interest are function of this coordinates it will be easy to compare different terms in the governing equations and thus obtain relevant regimes for the considered flows. The spatial coordinates take the form:

$$X'_M = \frac{X}{l_m} = \frac{\varepsilon^2 X}{h_{sc}} = \varepsilon^2 x' \tag{2.22}$$
$$X'_{sP} = \frac{X}{L_{sp}} = \frac{\varepsilon^3 X}{h_{sc}} = \varepsilon^3 x' \tag{2.23}$$

where x' is the coordinate non-dimensionalized by h_{sc}. Here the primes denote the non-dimensional variables and will be dropped hereafter. Using these new coordinates (the same procedure is applied for the time coordinates), we choose a multiple scales asymptotic ansatz for the unknown variables in the governing equations:

$$\boldsymbol{U}(t, \boldsymbol{x}, z; \varepsilon) = \sum_i \varepsilon^i \boldsymbol{U}^{(i)}(\varepsilon^2 t, \varepsilon^3 t, \varepsilon^2 \boldsymbol{x}, \varepsilon^3 \boldsymbol{x})\,, \tag{2.24}$$

where $\boldsymbol{U} = (p, \rho, \theta, \boldsymbol{u}, w)$. Variations of $\boldsymbol{U}$ on the following time and space scales are described with this expansion:

Mesoscale advection time :	$T_M = \varepsilon^2 t$	$0.5 \ldots 4$ days
Mesoscale :	$\boldsymbol{X}_M = \varepsilon^2 \boldsymbol{x}$	$200 \ldots 1800$ km
Seasonal time scale :	$T_{sea} = \varepsilon^3 t$	$4 \ldots 34$ days
sub-Planetary length scale :	$\boldsymbol{X}_{sP} = \varepsilon^3 \boldsymbol{x}$	$1800 \ldots 14000$ km

Table 2.3: Length and time scales of the expansion

A priori assumptions

In the asymptotic expansion, we suppose that the deviations from a constant reference value Θ_{ref} of the potential temperature θ are of the order ε^2. This is justified from measurements of the stratification of the atmosphere, given through the Brunt-Väisälä frequency N. Typical

values of N are $\sim 2 \times 10^{-2}\,\mathrm{s}^{-1}$. If we non-dimensionalize N using our reference length and velocity we obtain:

$$\left(\frac{l_{ref}N}{v_{ref}}\right)^2 \sim \left(\frac{10^4 \times 2 \times 10^{-2}}{5}\right)^2 \sim 100 \sim \varepsilon^{-2}$$

or using the definition of N:

$$\left(\frac{l_{ref}N}{v_{ref}}\right)^2 = \frac{g}{\Theta}\frac{\partial\theta}{\partial z}\frac{l_{ref}^2}{v_{ref}^2} \sim \frac{g}{h_{sc}}\frac{\delta\theta}{\Theta_{ref}}\frac{h_{sc}^2}{v_{ref}^2}$$

Thus we can estimate for the background stratification of the atmosphere

$$\frac{\delta\theta}{\Theta_{ref}} \sim \varepsilon^2\,. \tag{2.25}$$

Using Θ_{ref} as a reference temperature and non-dimensionalizing by it, the expansion for potential temperature takes the form

$$\theta = 1 + \varepsilon^2\Theta_2(z) + \varepsilon^3\theta^{(3)} + \mathcal{O}(\varepsilon^4)\,. \tag{2.26}$$

2.5 Derivation and results

In this section we describe briefly some steps in the derivation of the reduced model equations, using the asymptotic approach. Some intermediate results will be discussed.

First the partial derivatives can be written (applying the chain rule) as

$$\partial_t = \varepsilon^2\partial_{T_M} + \varepsilon^3\partial_{T_{sea}}$$
$$\nabla = \varepsilon^2\nabla_M + \varepsilon^3\nabla_{sP}$$

After the considerations above the derivation is straight forward: we take our ansatz (2.24) and substitute it in the governing equations (2.14) – (2.17).

For the zero order **Continuity equation** we obtain:

$$\mathcal{O}(\varepsilon^0): \qquad \partial_z\rho^{(0)}w^{(0)} = 0 \tag{2.27}$$

Integration gives for $z \to \infty$ and $\rho \to 0 \quad w^{(0)}(\infty) \to \infty$ which is not physical. So we require $w^{(0)} = 0$. Analogous it can be shown from the next order equation: $w^{(1)} = 0$. The next order gives:

$$\mathcal{O}(\varepsilon^2): \qquad \nabla_{\mathrm{M}} \cdot \boldsymbol{u}^{(\mathbf{0})} + \frac{1}{\rho_0}\partial_z \rho^{(0)} w^{(2)} = 0. \tag{2.28}$$

This equation expresses the inelastic approximation – since no density fluctuations are allowed, the sound waves are filtered. From the **vertical momentum balance** it follows that the atmosphere is in hydrostatic balance up to the order $\mathcal{O}(\varepsilon^3)$:

$$\partial_z p^{(i)} = -\rho^{(i)}, \quad i = 0, \ldots 3 \tag{2.29}$$

The expansion of the **potential temperature $\boldsymbol{\theta}$** gives:

$$\mathcal{O}(\varepsilon^0): \qquad \rho^{(0)} = {p^{(0)}}^{\frac{1}{\gamma}} \tag{2.30}$$

Using the hydrostatic balance:

$$p^{(0)}(z) = p_\infty \left(1 - \frac{\gamma - 1}{\gamma} z\right)^{\frac{\gamma}{\gamma - 1}} . \tag{2.31}$$

p_∞ is set to 1, because it is used as reference pressure. For the density we obtain $\rho^{(0)} = \rho^{(0)}(z)$ and $\rho^{(1)} = 0$. The next order potential temperature equation is:

$$\mathcal{O}(\varepsilon^2): \qquad \sum_{i=o}^{2} \rho^{(2-i)}\theta^{(i)} = {p^{(o)}}^{\frac{1}{\gamma}} \left(\frac{p^{(2)}}{\gamma p^{(0)}} + \frac{(1-\gamma)}{2\gamma^2}\frac{{p^{(1)}}^2}{{p^{(0)}}^2}\right) \tag{2.32}$$

Using

$$\partial_z \rho^{(0)} = -\frac{{\rho^{(0)}}^2}{\gamma p^{(0)}} \tag{2.33}$$

leads to:

$$\partial_z \pi^{(2)} = \theta^{(2)}, \quad \pi^{(i)} = \frac{p^{(i)}}{\rho^{(0)}} . \tag{2.34}$$

Similarly

$$\mathcal{O}(\varepsilon^3): \quad \partial_z \pi^{(3)} = \theta^{(3)} , \tag{2.35}$$

$$\mathcal{O}(\varepsilon^4): \quad \partial_z \pi^{(4)} = \theta^{(4)} + \frac{\gamma - 1}{2}(p^{(2)}(z))^2 . \tag{2.36}$$

From **the potential temperature transport** equation it follows:

$$S_\theta^{(i)} = 0, \quad i = 0, \ldots, 3\,. \tag{2.37}$$

In the next order we obtain **the weak temperature gradient approximation** (Sobel et al., 2001; Bretherton and Sobel, 2003)

$$\mathcal{O}(\varepsilon^4): \qquad w^{(2)} \frac{d}{dz}\Theta_2 = S_\theta^{(4)} \tag{2.38}$$

This equation expresses the fact that in the tropics the temperature distribution is horizontally uniform, which agree well with the observations (Holton, 1992). It states that diabatic heating will create vertical velocities. Air parcels will ascent adiabatically, thus experiencing cooling, which will compensate the heating when they reach their level of neutral buoyancy. The WTG approximation brings mathematical simplifications since we have a diagnostic algebraic equation for the vertical velocity.

The WTG approximation brings also simplifications in the applications on models with moisture budget (see: Bretherton and Sobel, 2002), for example on the QTCM's (quasi-equilibrium tropical circulation models).

The next order potential temperature equation has the form

$$\mathcal{O}\big(\varepsilon^5\big): \qquad \partial_{T_M}\theta^{(3)} + \boldsymbol{u}^{(0)} \cdot \nabla_{\mathrm{M}}\theta^{(3)} + w^{(2)}\partial_z\theta^{(3)} + w^{(3)}\frac{d}{dz}\Theta_2 = S_\theta^{(5)} \tag{2.39}$$

From **the horizontal momentum balance** we obtain for the leading orders

$$\nabla_{\mathrm{M}}\pi^{(i)} = 0, \quad i = 0, 1, 2 \tag{2.40}$$

$$\nabla_{\mathrm{sP}}\pi^{(i)} = 0, \quad i = 0, 1, 2 \tag{2.41}$$

$$\mathcal{O}(\varepsilon): \qquad \nabla_{\mathrm{M}}\pi^{(3)} = \boldsymbol{S}_{\boldsymbol{u}}^{(1)} \tag{2.42}$$

In Section 3.3 we will estimate the magnitude of the source term and show that $\boldsymbol{S}_{\boldsymbol{u}} \sim \mathcal{O}(\varepsilon^2)$. Thus we have

$$\boldsymbol{S}_{\boldsymbol{u}}^{(i)} = 0, \quad i = 0, 1 \tag{2.43}$$

The $\mathcal{O}(\varepsilon^2)$ momentum equation has then non-trivial form

$$\begin{aligned} \mathcal{O}(\varepsilon^2): \qquad & \partial_{T_M}\boldsymbol{u}^{(0)} + \boldsymbol{u}^{(0)} \cdot \nabla_{\mathrm{M}}\boldsymbol{u}^{(0)} + w^{(2)}\boldsymbol{u}_z^{(0)} + \beta Y_M \boldsymbol{k} \times \boldsymbol{u}^{(0)} \\ & + \nabla_{\mathrm{M}}\pi^{(4)} + \nabla_{\mathrm{sP}}\pi^{(3)} = \boldsymbol{S}_{\boldsymbol{u}}{}^{(2)} \end{aligned} \tag{2.44}$$

Equation (2.44) shows that on the scales considered here we do not have geostrophic flow in the tropics as we would have in the mid-latitudes, because of the smallness of the Coriolis parameter. So the nonlinear advection terms become comparable with the pressure gradient force and the Coriolis force. In addition we have a time evolution on the smaller time scale T_M.

It is of interest whether the derived equations (2.35), (2.39), (2.28) and (2.44) contain gravity waves. We consider the case when $w^{(3)}$, $\theta^{(2)}$ and $\pi^{(4)}$ are known functions and the pressure gradient force on the sub-planetary scale $\nabla_{\text{sP}}\pi^{(3)}$ does not vanish. The hydrostatic balance (2.35) couples the pressure with the potential temperature $\theta^{(3)}$. But for $\theta^{(3)}$ we have a prognostic equation (2.39), which states that fluctuations of the potential temperature will produce vertical velocities $w^{(2)}$. This will lead through the continuity equation (2.28) to horizontal velocity fluctuations and at the end to changes of pressure gradient force $\nabla_{\text{sP}}\pi^{(3)}$ in (2.44). Thus gravity waves will be excited.

For the next order momentum equation we have

$$\begin{aligned}\mathcal{O}(\varepsilon^3): \qquad & \partial_{T_M}\boldsymbol{u}^{(1)} + \boldsymbol{u}^{(0)}\cdot\nabla_{\text{M}}\boldsymbol{u}^{(1)} + w^{(2)}\boldsymbol{u}_z^{(1)} + \boldsymbol{u}^{(1)}\cdot\nabla_{\text{M}}\boldsymbol{u}^{(0)} \\ & +\partial_{T_{Sea}}\boldsymbol{u}^{(0)} + \boldsymbol{u}^{(0)}\cdot\nabla_{\text{sP}}\boldsymbol{u}^{(0)} + w^{(3)}\boldsymbol{u}_z^{(0)} \\ & +\beta Y_M\boldsymbol{k}\times\boldsymbol{u}^{(1)} + \boldsymbol{i}w^{(2)} + \nabla_{\text{M}}\pi^{(5)} \\ & +\nabla_{\text{sP}}\pi^{(4)} = \boldsymbol{S_u}^{(3)}\end{aligned} \tag{2.45}$$

It is interesting to note that in the equation for the zonal momentum there is an additional contribution $\boldsymbol{i}w^{(2)}$ from the Coriolis term.

Waves with dispersion relation of barotropic Rossby waves are supported under the WTG approximation (Majda and Klein, 2003; Bretherton and Sobel, 2003). Using

$$(T_M, X_M, Y_M, \nabla_{\text{M}}) \to (t, x, y, \nabla)$$

the linearized (about a state of rest) source free version of the equations (2.44), (2.28) and (2.38) takes the form

$$\partial_t\boldsymbol{u}^{(0)} + \beta y\boldsymbol{k}\times\boldsymbol{u}^{(0)} + \nabla\pi^{(4)} + \nabla_{\text{sP}}\pi^{(3)} = 0 \tag{2.46}$$

$$\partial_x u^{(0)} + \partial_y v^{(0)} = 0 \tag{2.47}$$

$$w^{(2)} = 0\,. \tag{2.48}$$

If we take the curl of the momentum equation with ∇ and use (2.42) and (2.43), we obtain the vorticity equation

$$\partial_t \zeta + \beta v = 0\,. \tag{2.49}$$

From the divergence constraint we can introduce a stream function $\psi(x, y)$ with arbitrary vertical structure $A(z)$

$$u^{(0)} = -A(z)\partial_y \psi\,, \qquad v^{(0)} = A(z)\partial_x \psi\,. \tag{2.50}$$

Then the vorticity is given through

$$\zeta = A(z)\Delta\psi(x, y). \tag{2.51}$$

The vorticity equation takes the form

$$\partial_t \Delta\psi + \beta\partial_x \psi = 0\,. \tag{2.52}$$

It is solved with the ansatz

$$\psi = a\ exp[i(kx + ly - \omega t)] \tag{2.53}$$

So we obtain the dispersion relation of barotropic Rossby waves on a β-plane approximation (Holton, 1992)

$$\omega = \frac{-\beta k}{k^2 + l^2}\,. \tag{2.54}$$

These waves can have arbitrary vertical structure. Majda and Klein (2003) supposed interactions between them and planetary waves from the midlatitudes.

2.6 The sub-planetary equatorial WTG regime

In order to investigate flows in the near equatorial belt, Majda and Klein (2003) chose an anisotropic scaling (X_{sP}, Y_M) and derived the seasonal sub-planetary equatorial WTG regime (SPEWTG). Here we use the same anisotropic spatial scaling and are interested on variations on the longer time scale T_{Sea}. The difference is that we consider a source term $S_\theta^{(4)} \neq 0$, the physical motivation is presented in Chapter 1 and 3. In this case the velocities $v^{(0)}$ and $w^{(2)}$ are not vanishing and we obtain significantly different system of equations. We replace:

$$\begin{gathered}(u^{(0)}, v^{(0)}, w^{(2)}, \rho^{(0)}) \to (u, v, w, \rho)\\ (S_u^{(2)}, S_v^{(2)}, S_\theta^{(4)}) \to (S_u, S_v, S_\theta)\\ (X_{sP}, Y_M) \to (x, y)\end{gathered}$$

Then the governing equations become

$$\mathcal{O}(\varepsilon^2): \qquad v\partial_y u + w\partial_z u - \beta y v + \partial_x \pi^{(3)} = S_u\,, \tag{2.55}$$

$$\mathcal{O}(\varepsilon^2): \qquad v\partial_y v + w\partial_z v + \beta y u + \partial_y \pi^{(4)} = S_v\,, \tag{2.56}$$

$$\mathcal{O}(\varepsilon^2): \qquad \partial_y v + \frac{1}{\rho}\partial_z \rho w = 0\,, \tag{2.57}$$

$$\mathcal{O}(\varepsilon^4): \qquad w\frac{d}{dz}\Theta_2 = S_\theta\,. \tag{2.58}$$

This system of equations describes a steady-state regime with zonal variations on a sub-planetary scale and meridional variations on a mesoscale (see Table 2.3). It includes the WTG approximation and a nondivergent constraint on the flow in the y, z-plane. The momentum equations have important nonlinear transport terms (see Section 1.4) and we have not a geostrophic motion. In order to obtain a closed system of equations, $d\Theta_2/dz$ (the stratification) and $\partial_x \pi^{(3)}$ have to be prescribed, for example from observational records. Then the vertical and the meridional velocities will have the same zonal structure as the source term S_θ. If we average the zonal momentum balance over x, the pressure gradient vanishes and the equations describe a steady-state zonally symmetric circulation

$$v\partial_y u + w\partial_z u - \beta y v = S_u\,, \tag{2.59}$$

$$v\partial_y v + w\partial_z v + \beta y u + \partial_y \pi^{(4)} = S_v\,, \tag{2.60}$$

$$\partial_y v + \frac{1}{\rho}\partial_z \rho w = 0\,, \tag{2.61}$$

$$w\frac{d}{dz}\Theta_2 = S_\theta\,. \tag{2.62}$$

This system is a $2D$ model of a circulation in the $y,\ z$ plane. In Fig. 2.1 we sketched a streamline of this circulation and in Fig. 2.2 a $3D$ trajectory of an air parcel. The direction of the flow depends on S_θ. We will study the simple case with a top-hat function as an externally imposed heat source, see Section 3.2. Some analytical and numerical solutions, describing the response of the atmosphere to such forcing, will be presented in Chapters 4, 5. In Schneider (1977) one can find the generalization of (2.59)-(2.62) for a zonally symmetric steady circulation on a sphere. Using scale analysis, the author there supports the WTG approximation (2.62), but he neglects the advection of meridional velocity (2.60). The latter was retained in the model equations for a Boussinesq fluid on a sphere by Held and Hou (1980), but they also allowed a meridional advection of potential temperature. Both studies are described briefly in Section 1.3.

We try to analyze how the zonally symmetric circulation will be modified by the term $\partial_x \pi^{(3)}$ in (2.55). We assume that we can prescribe the zonal pressure gradient force, then it can be regarded as a source term and the system of equations (2.55)-(2.58) has the same structure as (2.59)-(2.62). For simplicity we choose that $\partial_x \pi^{(3)}$ depends only on z. Due to the conservation of zonally averaged momentum the pressure gradient force in the upper atmosphere has to be equal and opposed to this in the lower atmosphere. So an air parcel moving poleward in the upper atmosphere will experience an additional acceleration e.g. in positive x-direction. When this parcel returns equatorward near the surface, it will be displaced in the negative x-direction. Thus the trajectory from Fig. 2.2 will be deformed, although it will remain helical.

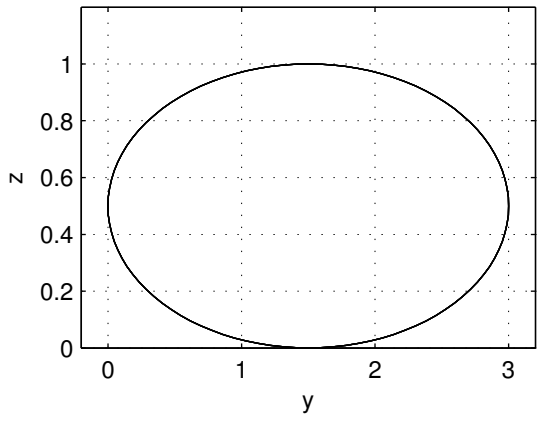

Figure 2.1: A stream line of the zonally averaged circulation

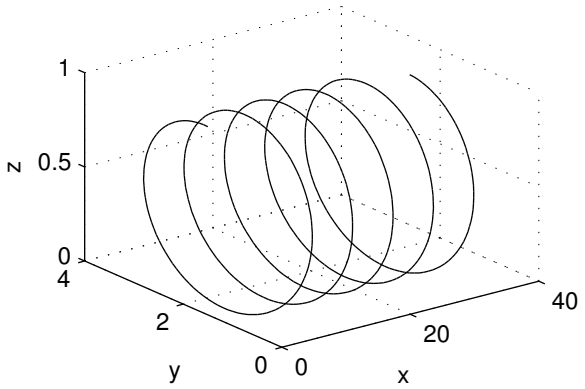

Figure 2.2: A trajectory of an air parcel

Chapter 3

Source Terms

In this Chapter we deal with the unresolved processes in the reduced equations, derived in Chapter 2. We analyze the important phenomena for the dynamics and propose different parameterizations.

There are two major diabatic processes that must be represented in the equation for the potential temperature: the release of latent heat due to the condensation of water vapor and the radiative cooling of the air.

3.1 Radiative processes

In our model we assume that there is no latitudinal variation of the incoming solar radiation so the atmospheric radiative equilibrium temperature is not dependent on the latitude. Scale analysis of the radiative source term shows that such variations will be not sufficient to produce a source term of the order ε^4.

Consider a simple relaxation ansatz for the source term due to radiation cooling:

$$S_\theta = \frac{\Theta_e - \Theta}{\tau} \tag{3.1}$$

Such an ansatz is a linearization about a state of radiative equilibrium of the atmosphere. Here τ is the radiative relaxation time scale with an empirical value of $\sim$ 20 days, and Θ_e denotes the radiative equilibrium temperature of the atmosphere. In Schneider and Lindzen (1977) and Held and Hou (1980) following distribution of Θ_e for a sphere was used

$$\Theta_e = \Theta_{ref}\left(1 - \Delta_h \sin^2\varphi + \Delta_v(\frac{z}{h_{sc}} - \frac{1}{2})\right) , \tag{3.2}$$

where φ denotes the latitude, $\Theta_{ref} = 300\,\mathrm{K}$ and $\Delta_h \sim \frac{1}{3}\ldots\frac{1}{6}$, and $\Delta_v \sim \frac{1}{8}$ is the fractional potential temperature drop from the equator to the pole and from the top of the atmosphere to the surface, respectively. If we use the β-plane approximation and the same scaling as for the

sub-planetary equatorial WTG regime (with $y_m = \varepsilon^2 y$) then in non-dimensional form (3.2) can be written as

$$\Theta_e^* = 1 - \Delta_h \varepsilon^2 y_m + \Delta_v (z - \frac{1}{2}) \tag{3.3}$$

Then we nondimensionalize (3.1) using our reference values for the temperature and the time (see Table 2.2).

$$S_\theta^* = \frac{t_{ref}}{\Theta_{ref}} S_\theta = \frac{t_{ref}}{\Theta_{ref}} \frac{\Theta_{ref}(\Theta_e^* - \Theta^*)}{\varepsilon^{-3} t_{ref} \tau^*} = \varepsilon^3 \frac{\Theta_e^* - \Theta^*}{\tau^*} \,. \tag{3.4}$$

The stars denote the non-dimensional variables of order one and hereafter will be dropped.

If we substitute now (3.3) and the expansion of θ in the equation above, we obtain

$$S_\theta = \varepsilon^3 \frac{\Delta_h \varepsilon^2 y_m + \Delta_v (z - \frac{1}{2}) - (\varepsilon^2 \Theta_2 + \varepsilon^3 \theta^{(3)} + \mathcal{O}(\varepsilon^4))}{\tau^*} \,. \tag{3.5}$$

It is of interest if such ansatz can produce a source term of order $\mathcal{O}(\varepsilon^4)$. This will happen only if the fluctuations of Θ_e and Θ are of the same order. The meridional variation of Θ_e is given through $\Delta_h \varepsilon^2 y_m$ and is $\mathcal{O}(\varepsilon^3)$. They are balanced by $\theta^{(3)}$ and will produce a source term $S_\theta^{(6)}$. For the vertical departures of the potential temperature we obtain that $\varepsilon^2 \Theta_2$ must be balanced by $\Delta_v (z - \frac{1}{2})$. But this will give a source term $S_\theta^{(5)}$.

The consideration above shows that radiative processes are not sufficient to drive a circulation given by (2.59)-(2.62) (on the spatial scales of interest). This is also supported if we take a typically value for the rate of cooling, due to long wave emission. In Gill (2003) and Holton (1992) one can find $S_{rad} \sim 1$ K day^{-1}, or in nondimensional form

$$S_{rad} \frac{t_{ref}}{\Theta_{ref}} \sim 1 \frac{K}{\varepsilon^{-2} t_{ref}} \frac{t_{ref}}{\Theta_{ref}} \sim \varepsilon^5 \tag{3.6}$$

This estimates lead to the conclusion that $S_\theta^{(4)} = 0$ in the equation for the potential temperature (2.62), when only radiative processes are included. But this implies $v^{(0)} = w^{(0)} = 0$ and from the meridional momentum balance

$$\beta y u^{(0)} = \partial_y \pi^{(4)} \,. \tag{3.7}$$

This solution is not appropriate for the tropical zone, because of violation of the momentum equation in the presence of viscosity: see Section 4.4. But it can be applied for the higher latitudes. We consider the next order of the governing equations – (2.45), (2.39). The source term $S_\theta^{(5)}$ will drive a weak meridional circulation $(v^{(1)}, w^{(3)})$ superposed on the geostrophically balanced zonal wind $u^{(0)}$, disturbed through $u^{(1)}$. The polar cell will be an example of such weak thermally driven circulation. The numerical simulations of Schneider and Lindzen (1977) and Schneider (1977) showed also that in the presence of a radiative source term only, the Hadley cell will be a tiny part of the observed mass overturning.

A more sophisticated parameterization of the radiative processes will be achieved if we split the source term in contributions from incoming shortwave solar radiation and outgoing terrestrial longwave radiation (Petoukhov et al., 2003). Then the longwave radiation fluxes can be calculated, taking into account temperature and moisture distribution or even concentration of CO_2, methane, water vapor and other greenhouse gases in the atmosphere. The same can be made for the short wave radiation, which is influenced through absorption of ozone and aerosols and albedo effects (e.g. albedo of the clouds).

In our simplified model the radiative parameterization will be kept as simple as possible. The reason is the inferior role of the radiative processes in driving the tropical circulation on the considered length scales.

3.2 Convection

The previous section shows that there must be another mechanism for the production of the available potential energy, which drives the observed Hadley circulations.

We consider a convecting atmosphere. In the hot towers of the ITCZ large amounts of latent heat are released due to condensation, thus producing a diabatic source term in (2.62). We try to estimate it. Typically precipitation rates in the tropics are of the order $2\,\mathrm{cm\ day}^{-1}$ which corresponds to the condensation of $20\,\mathrm{kg}$ water in an air column of $1\,\mathrm{m}^2$ cross section (Holton, 1992). The condensation of this water will increase on average $5\,\mathrm{K\ day}^{-1}$ the temperature of the air. The vertical distribution of the heating has maximum in the middle atmosphere, reaching a rate of $10\,\mathrm{K\ day}^{-1}$. In non-dimensional form this gives a source term

$$S_{con}\frac{t_{ref}}{\Theta_{ref}} \sim \varepsilon^4 \tag{3.8}$$

This estimate shows that the process of latent heat release will be mainly responsible for the source term in the potential temperature equation. The question remains how to parameterize it.

If we use a relaxation ansatz, the convective adjustment time scale τ_{con} will be of the order $\sim \mathcal{O}(30\,\mathrm{min})$. Then we have to give appropriate equilibrium temperature profile but this is not an easy task (as for the radiation equilibrium temperature), since this profile will be dependent on the interactions with the large-scale flow (see the parameterization of S_θ using water vapor budget). Another important aspect is that the convection itself has different feedbacks with the subcloud mixed layer (for example through downdraughts). Thus it changes the static energy and water vapor content there, which on the other hand controls the evolution of the convection (see Section 1.2). If we follow this approach and try to capture the complex interactions in a convective atmosphere, this will lead to additional nonlinear terms in our system of equations (2.59)-(2.62). To go round this problem, we will not consider the interactions, keeping the system as simple as possible by prescribing the source term S_θ. Suppose it can be written as

$$S_\theta = M(y)Z(z) \tag{3.9}$$

To represent the release of latent heat in the ITCZ, which is a narrow belt around the globe (see Fig. 1.1), we use a top-hat function for the meridional distribution $M(y)$ with $Y_m \ll Y_h$

$$M(y) := \begin{cases} H_e & \text{for } y \leq Y_m \\ H_0 & \text{for } Y_m < y < Y_h \\ 0 & \text{else} \end{cases} . \tag{3.10}$$

Y_h denotes the boundary of the Hadley circulation which will be established and the region of cumulus heating is between 0 and Y_m because $H_e > 0$. Here we consider only the northern hemisphere because of symmetry. The function $M(y)$ is sketched out in Fig. 4.1. The area of positive M represents heating due to deep cumulus convection and this of negative M - cooling due to longwave emission of the air. Since the contribution of the radiative processes is an order of magnitude smaller then those of the convective, we have $|H_e| \gg |H_0|$. The width of the forcing region is Y_h and is determined from the constraint $\int S_\theta \mathrm{d}y = 0$ (see Section 3.2.2). Note, that we have made the additional assumption that the heating is centered symmetrically around the equator (which is not always true for the ITCZ), in order to study some general features of the sub-planetary equatorial regime. Similar top-hat source term was used by Sobel et al. (2001) and Polvani and Sobel (2002). Schneider and Lindzen (1977) and Schneider (1977) used a narrow Gaussian type curve to represent the distribution of the heating. If we subtract from it the contribution of the radiative processes (meridional uniform on the l_m scale) we obtain similar S_θ as (3.10). Finally we have also studied the case when the source term is given through a smooth function like $\tanh$, see Chapter 4, but no significant differences were observed.

Next we have to specify the vertical distribution of S_θ. $Z(z)$ has similar profile as the large scale vertical mass flux. From (2.62) it follows that the source term reaches its maximum, where the largest vertical velocities occur - in the divergence-free level. Observations indicate that the mean height of this level lies at $\sim$ 500 mb (Gill, 2003) or between $400 - 300$ mb (Holton, 1992). Schneider and Lindzen (1977) assume that for a non-entraining cumulus tower $Z(z)$ will be constant from 800 mb to 200 mb and decrease linearly to zero at 100 mb (the decrease corresponds to the detrainment near the tropopause). In the general case the vertical distribution of S_θ depends on the height of the clouds in the convecting region, their cross section and so on. In the parameterization schemes sub-ensembles are introduced, they contain clouds with similar properties e.g. the same cloud height, fractional entrainment rate. An example of such sophisticated approach are the Betts-Miller or Arakawa-Schubert convecting schemes.

In our study we have used a vertical distribution proposed by Gill (1980)

$$Z(z) = \sin \pi z \, . \tag{3.11}$$

This is a first order approximation to the observations of latent heating in convecting systems and it satisfies the condition of disappearing vertical velocity at the top and the ground. More realistic profile will be achieved if we include a $\beta e^{-\alpha z}$ dependence in $Z(z)$. The choice of the constants α and β will control the magnitude and the position of the latent heating in the vertical direction. Thus the distribution of $Z(z)$ can be matched to observational profiles.

An interesting feature of (3.11) is that this distribution of heating will excite only the first baroclinic mode and then the problem can be reduced to solving the shallow water equations

(Gill, 1980). Using a separation of variables technique the 3D compressible flow equations for a stable stratified fluid can be written as a set of shallow water equations with different equivalent depths, corresponding to different normal modes. Gill (1980) showed that the linearized SW equations have steady-state solutions, representing the Hadley and the Walker circulations.

3.2.1 Parameterization of S_θ using water vapor budget

One approach to parameterize the source term of the potential temperature is to use a water vapor budget for closure (Kuo, 1974). This ansatz has been criticized because the potential temperature source term is regarded as an external heating and many interactions in the atmosphere are not considered. But we will present it as the simplest way to describe the processes between the convecting system and the large-scale flow and because it has been used in many models of the tropical circulation (Wang and Li, 1993).

The key idea is that since there is no sufficient storage of water in the clouds, the precipitation P over some area will be the sum of the surface evaporation E and the large-scale moisture convergence

$$P = -\int_0^{z_a} \nabla_h \cdot \rho q \boldsymbol{v} \mathrm{d}z + E\,. \tag{3.12}$$

Here q denotes the specific humidity and $z_a \sim 2\,\mathrm{km}$ corresponds to the height of the trade inversion in the tropics, the main amount of water vapor in the atmosphere is stored below it. To find the integrated over an air column heating, we have to multiply the precipitation by the latent heat of condensation $L_c \sim 2.5 \times 10^6\,\mathrm{J\,kg^{-1}}$

$$\int_0^1 S_{con} \mathrm{d}z = bL_cP\,. \tag{3.13}$$

S_{con} denotes the release of latent heat and $b \sim 0.75$ gives the efficiency of the condensation heating. Implying that the moisture convergence does not change significantly q (Holton, 1992), the continuity equation for the water vapor takes the form

$$\nabla_h \cdot \rho q \boldsymbol{v} + \partial_z \rho q w = 0\,. \tag{3.14}$$

We have neglected horizontal turbulent transport as well as source terms of q. Substituting this in (3.12) yields

$$P = \rho q w\Big|_{z_a} + E\,, \tag{3.15}$$

where we have used the boundary condition of vanishing vertical velocity at the surface. Finally, we have for the latent heating

$$S_{con} = Z_n(z) b L_c \left(\rho q w\Big|_{z_a} + E\right)\,. \tag{3.16}$$

The function $Z_n(z)$ gives the vertical distribution of the heating and has the constraint

$$\int_0^1 Z_n(z)\mathrm{d}z = 1 \tag{3.17}$$

Using the bulk transfer approach (Peixoto and Oort, 1992), we have for the surface evaporation

$$E = -\rho C_w |\boldsymbol{v}_a|(q_a - q_s)\,, \tag{3.18}$$

where $\boldsymbol{v}_a$, and q_a are the velocity and the specific humidity of the air evaluated at $\sim 10\,\mathrm{m}$ height, respectively. q_s is evaluated at the surface $z = 0$. C_w is the bulk transfer coefficient of water vapor and is dimensionless. For the ratio between the sensible heat flux H and the latent heat flux at the surface L_eE ($L_e = L_c$ is the latent heat of evaporation) we have

$$B = \frac{H}{L_e E}\,. \tag{3.19}$$

This is the Bowen ratio. Both fluxes can be given from the flux-gradient approach as

$$H = -K_H \rho c_p \frac{\partial \theta}{\partial z} \tag{3.20}$$

and

$$E = -K_w \rho \frac{\partial q}{\partial z}\,, \tag{3.21}$$

where K_h and K_w are the eddy diffusivity coefficients for sensible heat and water vapor ($K_H = K_w$). Substituting the representations of the fluxes in (3.19) gives

$$B = \frac{c_p}{L_c}\frac{\frac{\partial\theta}{\partial z}}{\frac{\partial q}{\partial z}} = \frac{c_p}{L_c}\frac{\partial\theta}{\partial q} \sim \frac{c_p}{L_c}\frac{\Delta\theta}{\Delta q}\,. \tag{3.22}$$

Using this relation the evaporation (3.18) can be expressed in terms of the temperature

$$E = -\rho c_p \frac{C_w}{B L_c}|\boldsymbol{v}_a|(\theta_a - \theta_s)\,, \tag{3.23}$$

where θ_a is the potential temperature at $\sim 10\,\mathrm{m}$ and θ_s the surface temperature. For a model with a coarser resolution it will be difficult to give appropriate value for θ_a. In Wang and Li (1993) one can find more useful formulation for the evaporation. Suppose that the surface is covered by the ocean, then q_s will be equal to the saturation specific humidity q_{sat} and we have

$$E = \rho C_w |\boldsymbol{v}_a|(q_{sat} - q_a)\,. \tag{3.24}$$

Wang and Li (1993) use a empirical formula for $q_a(T)$ as a function of the surface temperature T_s

$$q_a = 10^{-3}\left(18 + 0.67\ K^{-1}(T_s - 300\ K)\right) \tag{3.25}$$

The dependence of q_{sat} on the temperature T can be obtain from the Clausius-Clapeyron equation (Peixoto and Oort, 1992) for the water vapor saturation pressure $e_{sat}(T)$

$$\frac{de_{sat}}{dT} = \frac{L_c}{T(\alpha_v - \alpha_w)}\,, \tag{3.26}$$

where α_w, and α_v are the specific volumes of water in fluid and gaseous phase, respectively. Under the approximation that water vapor at the saturation pressure behaves like an ideal gas, we can write for α_v

$$e_{sat}\alpha_v = R_v T\,. \tag{3.27}$$

Here R_v is the gas constant of water vapor. Using this equation and taking into account that $\alpha_w \ll \alpha_v$ in (3.26), we obtain

$$\frac{de_{sat}}{dT} = \frac{L_c e_{sat}}{R_v T^2}\,. \tag{3.28}$$

We can write an ideal gas equation also for the dry air with the pressure p_d, specific volume α_d and gas constant R_d

$$p_d\alpha_d = R_d T\,. \tag{3.29}$$

Then from (3.27) and (3.29) q_{sat} can be expressed as

$$q_{sat} = \frac{\alpha_d}{\alpha_v + \alpha_d} = \frac{R_d}{R_v}\frac{e_{sat}}{p_d + \frac{R_d}{R_v}e_{sat}} \approx\ 0.622\frac{e_{sat}}{p}\,, \tag{3.30}$$

where $p = p_d + e_{sat}$ and $R_d/R_v \approx 0.622$. Substituting (3.30) in (3.28) we obtain

$$\frac{dq_{sat}p}{dT} = \frac{L_c q_{sat} p}{R_v T^2}\,. \tag{3.31}$$

We try to estimate the magnitude of the the pressure fluctuations due to temperature changes. For this purpose we rewrite the above equation

$$\frac{dq_{sat}}{dT} = \frac{L_c q_{sat}}{R_v T^2} - \frac{q_{sat}}{p}\frac{dp}{dT}\,, \tag{3.32}$$

or using reference quantities

$$\frac{\delta q}{\delta T}\frac{dq^*_{sat}}{dT^*} = \frac{L_c \bar{q}_{sat} q^*}{R_v T^2_{ref} T^{*2}} - \frac{q^*_{sat}}{p^*}\frac{\bar{q}_{sat}}{p_{ref}}\frac{\delta p}{\delta T}\frac{dp^*}{dT}\,. \tag{3.33}$$

Here $\bar{q}_{sat}$ is the reference saturation specific humidity and the stars denote non-dimensional variables of the order one. If we substitute appropriate values we obtain the scaling

$$\frac{L_c}{R_v T_{ref}} \sim 18.5 \sim \frac{C^*}{\varepsilon}\,. \tag{3.34}$$

In (Emanuel, 1994, p. 7) one can find the following useful estimate for the pressure fluctuations

$$\frac{\delta p}{p_{ref}} \sim \frac{u_{ref}}{\sqrt{p_{ref}/\rho_{ref}}} \sim \varepsilon^4\,. \tag{3.35}$$

where we have used the definition of the Mach number (2.6) and the scaling as in (2.9). Substituting this in (3.33) we finally obtain

$$\frac{\delta q}{\bar{q}_{sat}}\frac{dq^*_{sat}}{dT^*} = \frac{\delta T}{T_{ref}}\frac{C^* q^*}{\varepsilon T^{*2}} - \varepsilon^4 \frac{q^*_{sat}}{p^*}\frac{dp^*}{dT^*}\,. \tag{3.36}$$

Using a mean atmospheric lapse rate $\Gamma \sim 6\,\mathrm{K\ km^{-1}}$ in non-dimensional form we have

$$\frac{\delta T}{T_{ref}} = \frac{h_{sc}}{\Theta_{ref}} 6\ K\ km^{-1} \sim \frac{1}{5} \sim \varepsilon \tag{3.37}$$

The ratio $\delta q/\bar{q}_{sat}$ ranges from from 0 up to 1 since we can have a saturated air parcel or a dry one. Thus we estimate

$$\frac{dq^*_{sat}}{dT^*} = \frac{C^* q^*}{T^{*2}} - \varepsilon^4 \frac{q^*_{sat}}{p^*}\frac{dp^*}{dT^*}\,. \tag{3.38}$$

This equation states that the pressure fluctuations due to temperature changes are small. Thus we can integrate (3.31) from a reference temperature T_r to T, assuming that the pressure remains constant

$$q_{sat}(T) = q_{sat}(T_r)\mathrm{exp}[-\frac{L_c}{R_v T_r}\frac{T_r - T}{T}] \tag{3.39}$$

We are interested on the case when T is close to T_r. Then we can expand $q_{sat}(T)$ in a Taylor series about T_r providing that the exponent is small. Using the hydrostatic balance, the definition of the potential temperature (2.5) and the estimate (2.25), one finds the following representation of the temperature (Klein, unpublished notes on asymptotic scalings for moisture and latent heat)

$$T = 1 - \varepsilon \frac{\gamma - 1}{\gamma} z + \varepsilon^2 T^{(2)} + \mathcal{O}(\varepsilon^3)\,. \tag{3.40}$$

Since we are interested on the specific humidity at the ocean surface, we will set $z = 0$ and obtain

$$\frac{T_r - T}{T} \sim \varepsilon^2\,. \tag{3.41}$$

Using (3.34), we can say that the exponent in (3.39) is of the order ε. We rewrite the expression in a series

$$q_{sat}(T) \approx q_{sat}(T_r)\left(1 + \frac{L_c}{R_v T_r^2}(T - T_r)\right) \tag{3.42}$$

In Wang and Li (1993) one can find that substituting (3.25) and (3.42) with $T = T_s$ in (3.24) gives

$$E = \rho C_w |\boldsymbol{v}_a| K_q (T_s - T_*)\,, \tag{3.43}$$

where $T_* = 293.2\,\mathrm{K}$ and $K_q = 6.95\ 10^4\,\mathrm{K}^{-1}$. T_s is equal to θ_s at the sea level. This formula can be applied when the sea surface temperature exceeds $295.2\,\mathrm{K}$ and Wang and Li (1993) use it for the Pacific ocean between $30°N$ and $30°S$.

3.2.2 Constraint on the potential temperature source term

Since we are interested on steady-state circulations, the conservation of energy implies that the integral of S_θ over the whole domain of the circulation must disappear. Suppose we average in the vertical and meridional direction the equation for potential temperature, then it takes the form:

$$\overline{w^{(2)}} \frac{d}{dz}\Theta_2 = \overline{S_\theta^{(4)}} \tag{3.44}$$

Note that we have assumed for simplicity that the static stability $\frac{d}{dz}\Theta_2$ is constant. The bars denote an average over the area of the circulation when it is confined in y direction between 0 and Y and in z direction between 0 and Z

$$\overline{A} = \frac{1}{YZ} \int_0^Y \int_0^Z A\,\mathrm{d}y\mathrm{d}z\,. \tag{3.45}$$

If $\overline{S_\theta^{(4)}}$ does not vanish this would mean that there is a resulting vertical velocity $\overline{w^{(2)}}$ of the whole atmosphere which is not observed. So we will assume further $\overline{S_\theta^{(4)}} = 0$.

3.2.3 Static stability

In the potential temperature equation the term $\sigma = \frac{d}{dz}\Theta_2$ is often referred to as static stability and characterizes the stratification of the atmosphere. We have in dimensional form $\sigma_{dim} = \Theta/T(\Gamma_d - \Gamma)$, where Γ_d is the dry adiabatic lapse rate and Γ the real lapse rate of the atmosphere $\sim 6 - 7\,\mathrm{K\ km^{-1}}$. Typical value found in the literature for the static stability is $\sim 3\,\mathrm{K\ km^{-1}}$. If we nondimensionalize it we obtain

$$\sigma = \frac{h_{sc}}{\Theta_{ref}} 3\ K\ km^{-1} \sim \frac{1}{10} \sim \varepsilon^2 c \tag{3.46}$$

Where c is $\mathcal{O}(1)$ and we have used the same scaling for the background stratification as by the estimate made in Section 2.4, see also Majda and Klein (2003). For the numerical and analytical solutions c was set to 1.

3.3 The source terms $S_u,\ S_v$

S_u and S_v represent a sink in the zonal, meridional momentum equations. This can be due to viscous friction, small scale turbulence, large-scale eddies, non resolved vertical transport in the cumulus clouds and others.

For the analytical solution we use a Rayleigh friction, which is derived from a relaxation ansatz with zero equilibrium velocity

$$S_u = -\alpha u\,, \tag{3.47}$$

$$S_v = -\alpha v\,. \tag{3.48}$$

The same representation of the source term was used by Gill (1980) in his study of forced equatorial motions. It was also used by Sobel et al. (2001) to give some analytical solutions for a Hadley circulation derived from the shallow water equations under the WTG approximation. For simplicity we assume that α does not depend on z and y for the analytical solutions. One can find in Gill (1980) $\alpha = \frac{1}{2}\,\mathrm{day}^{-1}$. If we nondimensionalize the source term, we obtain

$$S_u \frac{h_{sc}}{u_{ref}^2} = \varepsilon^2 c\,, \tag{3.49}$$

where $c \sim \frac{1}{2}$ and the source term in the momentum balance is sufficiently strong - $\mathcal{O}(\varepsilon^2)$. Bretherton and Sobel (2003) pointed out that $\alpha \sim 0.5\,\mathrm{day}^{-1}$ is realistic only when boundary layer flow is simulated. It is a feature of the Gill-type models to have large damping rates in order to produce a circulation close to the observed. A realistic value of α in the upper atmosphere will be $\alpha \sim 0.1\,\mathrm{day}^{-1}$ or less. In the asymptotic we are interested in $\lim_{\varepsilon\to 0} S_u$ and it goes like $\varepsilon^2 c$, because of the large values of α in the boundary layer, even if we have $c(z \to 1) \to 0$ in the upper atmosphere.

Solutions has been computed with a more realistic source term representing turbulent mixing. The momentum source term is generally defined from the stress tensor $\vec{\vec{\boldsymbol{\tau}}}$:

$$\boldsymbol{S} = \frac{1}{\rho} \nabla \cdot \vec{\vec{\boldsymbol{\tau}}} \tag{3.50}$$

If we use the scaling proposed in Chapter 2 we have

$$\boldsymbol{S} = \frac{1}{\rho} \left(\varepsilon^2 \nabla_M \cdot \vec{\vec{\boldsymbol{\tau}}} + \varepsilon^3 \nabla_{sP} \cdot \vec{\vec{\boldsymbol{\tau}}} + \partial_z \boldsymbol{k} \cdot \vec{\vec{\boldsymbol{\tau}}} \right) . \tag{3.51}$$

So we have for the source term of zonal momentum in leading order:

$$S_u = \frac{1}{\rho} \partial_z \tau_{zx} + \mathcal{O}\left(\varepsilon^2\right) . \tag{3.52}$$

If we use a gradient parameterization of the shear stress: $\vec{\vec{\boldsymbol{\tau}}} = \mu \nabla \boldsymbol{u}$ where μ is a dynamic eddy coefficient, then we have

$$S_u = \frac{1}{\rho} \partial_z \mu \partial_z u \, . \tag{3.53}$$

For simplicity we assume here that μ is not a function of z, with $\nu = \frac{\mu}{\rho}$ we have for the non-dimensional form of (3.53)

$$S_u^* = S_u \frac{h_{sc}}{u_{ref}^2} = \nu_{ref} \frac{u_{ref}}{h_{sc}^2} \frac{h_{sc}}{u_{ref}^2} \nu^* \partial_{z'z'} u^* = \frac{1}{Re} \nu^* \partial_{z'z'} u^* \, , \tag{3.54}$$

where Re is the Reynolds number and the stars denote the non-dimensional variables and will be dropped hereafter. If we substitute our reference values for the turbulent kinematic viscosity (ν_{ref} ranges from $50\,\mathrm{m^2\,s^{-1}}$ in the boundary layer to $1\,\mathrm{m^2\,s^{-1}}$ in the free atmosphere) we obtain $Re \sim \mathcal{O}(\varepsilon^{-3}) \ldots \mathcal{O}(\varepsilon^{-4})$. This would mean that the momentum source is one to two orders weaker then the terms in (2.59) and (2.60). On the other hand in Chapter 5 we present some numerical solutions and show that the zonal wind speed can reach $\sim 100\,\mathrm{m\,s^{-1}}$. Using this value for reference velocity, one obtain a sufficiently strong momentum source term. Another aspect is that the parameterization (3.53) has to represent not only turbulence, but other forms of friction – for instance cumulus friction (see next paragraph for an explanation). In a convecting atmosphere this process is much effective by the dissipation of kinetic energy. Thus we will not neglect the momentum sink and set Re to be $\mathcal{O}(\varepsilon^{-2})$.

$$S_u = \frac{1}{Re} \tilde{c} = \varepsilon^2 \tilde{c} \, , \tag{3.55}$$

which is in accordance with (3.49), and we have $\tilde{c} \ll 1$ in the upper atmosphere.

When we consider convection, momentum transport in the cumulus towers plays an important role in the momentum balance (Schneider and Lindzen, 1977; Schneider, 1977). This

process is called cumulus friction, because air with nearly zero horizontal velocities from the ground is pumped in the upper troposphere and thus reducing the strong upper winds. A parameterization of this process can be found in Schneider and Lindzen (1976). The source term can be then expressed in terms of the mass flux M_{con}in the cumulus towers and the large-scale zonal velocities

$$S_u = \frac{1}{\rho}\partial_z \left(M_{con}(u - u_c) \right) . \tag{3.56}$$

To a first approximation u_c can denote the zonal velocity at cloud base. Using such parameterization the zonal momentum equation can be brought in a form similar to that with $S_u = -\alpha u$ and we can use the same techniques to find analytical and numerical solutions. But due to time constraints we have not dealt with this case.

The mass flux in the cumulus clouds can be derived from the heating

$$\frac{M_{con}}{\rho}\frac{d\Theta_2}{dz} = w'\frac{d\Theta_2}{dz} = S_{con} , \tag{3.57}$$

where w' is the averaged velocity in the clouds and S_{con} is the heating due to convection. If we prescribe the meridional distribution of S_θ (see (3.10)) we have

$$\int S_{con}\mathrm{d}z = \begin{cases} H_e + |H_0| & \text{for } y \leq Y_m \\ 0 & \text{else} \end{cases} . \tag{3.58}$$

For the definitions of H_e,H_0 and Y_m see the text below (3.10). In the vertical we can use the same distribution as for S_θ.

Chapter 4

Analytical Solutions

In this chapter a mass stream function is introduced and we present some analytical solutions for the meridional and vertical velocities. We discuss geostrophically balanced solutions in the context of Hide's theorem for a β-plane fluid.

4.1 The Stream function

Recall the governing equations (2.59)-(2.62), which have been derived in Chapter 2. From the continuity equation (2.61) it follows that the meridional mass transport is nondivergent in the z, y plane. We can introduce a mass stream function ψ which identically satisfies (2.61):

$$\partial_z \psi = -\rho v \,, \tag{4.1}$$

$$\partial_y \psi = \rho w \,. \tag{4.2}$$

If we differentiate (2.62) with respect to y and substitute (4.2) we have

$$\partial_{yy} \psi = \sigma^{-1} \rho \partial_y S_\theta, \tag{4.3}$$

where $\sigma = d\Theta_2/dz$. The stream function ψ can be represented using Fourier series in y and z (ψ must vanish outside the boundaries). To make a rough estimate, the second derivative of ψ with respect to y can be set proportional to $-\psi$, so we have

$$\psi \sim -\sigma^{-1} \rho \partial_y S_\theta \,. \tag{4.4}$$

Since we expect $\partial_y S_\theta < 0$ to be true for the earth - latent heating near the equator and radiative cooling in the upper latitudes, equation (4.4) states that the meridional gradient of the diabatic source term will drive a circulation with $\psi > 0$. This will be a thermally direct Hadley cell with ascending air near the equator and descending far from it as it can be seen from the definition of ψ (4.2). The vertical velocities will produce adiabatic cooling in the region of

rising motion (see (2.62)) and adiabatic heating elsewhere thus acting to reduce temperature differences in the atmosphere.

The stream function ψ can be computed analytically from (4.1), (4.2) using different representations of the source term $S_\theta = Z(z)M(y)$ (Section 3.2). For the vertical distribution we make the assumption $Z(z) = \sin(\pi z)$. Using (2.62) we obtain for the vertical velocity

$$w = \sigma^{-1} M(y) Z(z) \,. \tag{4.5}$$

We assume for simplicity that the term $d\Theta_2/dz$, representing the static stability of the atmosphere, is constant and will denote it by σ hereafter.

We consider the case when $M(y)$ is a top-hat function (3.10). Due to energy conservation, see Section 3.2.2, we have the constraint $\overline{S_\theta} = 0$, thus we obtain for H_0

$$H_0 = -\frac{Y_m H_e}{(Y_h - Y_m)} \,. \tag{4.6}$$

Fig. 4.1 illustrates the distribution of $M(y)$. For the particular choice of $M(y)$ the vertical velocity takes the form

$$w = \begin{cases} H_e \sigma^{-1} \sin(\pi z) & \text{for } |y| \le Y_m \\ H_0 \sigma^{-1} \sin(\pi z) & \text{for } Y_m < |y| < Y_h \\ 0 & \text{else} \,. \end{cases} \tag{4.7}$$

Substituting some appropriate values for H_e and σ (see Chapter 3) we obtain $w \sim 4\,\text{cm s}^{-1}$. This value agree well with observation of the vertical velocity in large-scale convecting regions $\sim 3\,\text{cm s}^{-1}$ (Holton, 1992). From (4.2) we have for the stream function

$$\psi = \begin{cases} y\rho w & \text{for } y \le Y_m \\ (Y_h - y)\rho w & \text{for } Y_m < y < Y_h \\ 0 & \text{for } y \ge 0 \,. \end{cases} \tag{4.8}$$

We have also made some experiments when $M(y)$ is a smooth function, see Fig. 4.1

$$M(y) = \begin{cases} c \tanh(b - dy) + a & \text{for } 0 \le y \le Yh \\ 0 & \text{else} \ . \end{cases} \tag{4.9}$$

We can prescribe the strength of the forcing as well as the position and the width of the transition region (where $M(y)$ has the greatest slope), choosing the parameters $b,\ c$ and d. Then a can be computed using the constraint $\overline{S_\theta} = 0$

$$a = \frac{c}{Y_h d} \ln \frac{\cosh(b - dY_h)}{\cosh(b)} \,. \tag{4.10}$$

The stream function is given by

$$\psi = \begin{cases} \sigma^{-}1\rho\sin(\pi z)\left(ay - \dfrac{c}{d}\ln\dfrac{\cosh(b-dy)}{\cosh(b)}\right) & \text{for } 0 < y < Y_h \\ 0 & \text{for } y \geq Y_h \end{cases} \tag{4.11}$$

The stream function is sketched out in Fig. 4.2.

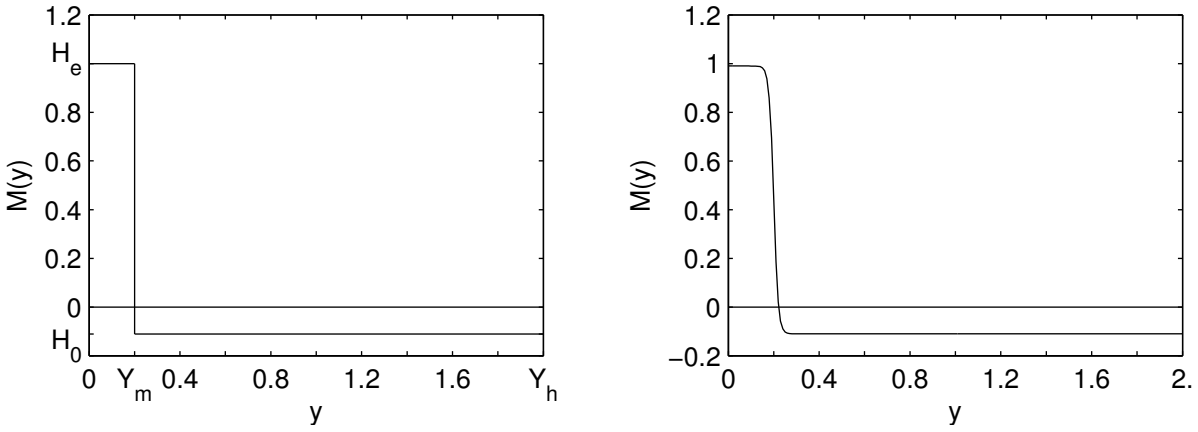

Figure 4.1: The forcing $M(y)$ a top-hat function (left) and a smooth function (right)

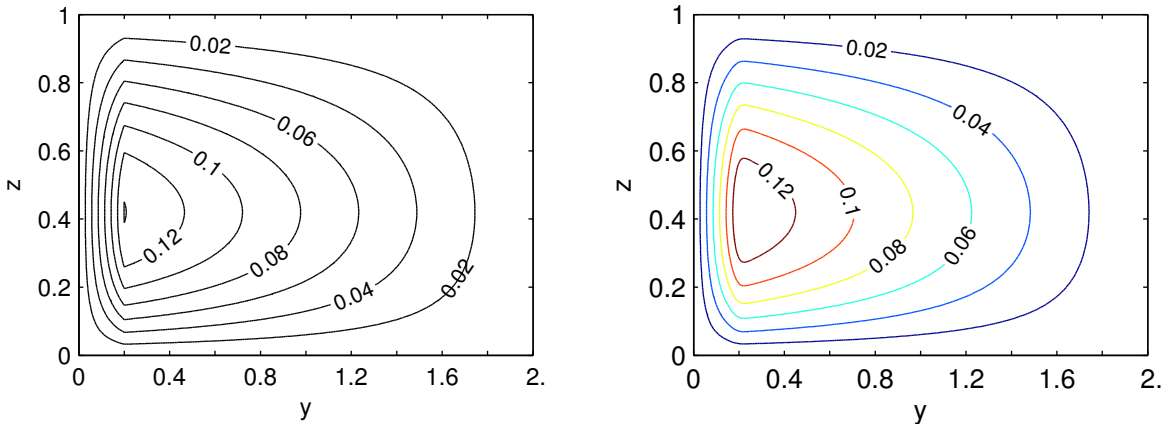

Figure 4.2: The Stream Function ψ for $M(y)$ a top-hat function (left) and a smooth function (right)

The direction of the flow is clockwise. Rising motions are confined in the belt $y < Y_m$, as it follows from (2.62). This area is an order of magnitude smaller than the region of descent, because of the different strength of the convective heating and the radiative cooling. There is no significant difference in the magnitude of ψ for both source functions. Note the kink in the stream lines in the left plot in Fig. 4.2, due to the discontinuity of $M(y)$ at Y_m. When the region of heating is comparable with this of the cooling the established circulation (Fig. 4.3) has the form of the seasonal mean Hadley cell (Fig 1.3).

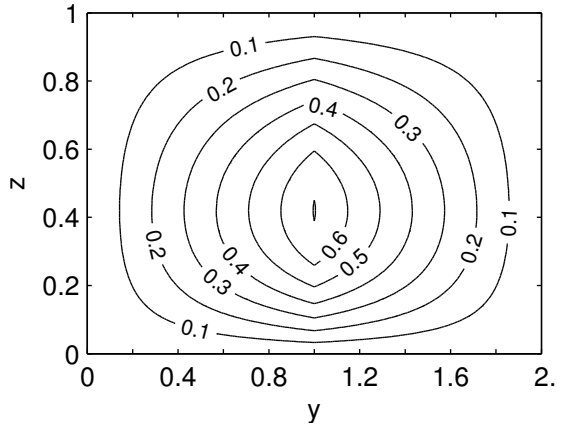

Figure 4.3: The Stream Function ψ for $M(y)$ a top-hat function and $Y_m = 1$.

From (2.61) we can give an analytical expression for the meridional velocity

$$v = -\frac{1}{\rho\sigma}\partial_z \rho Z(z) \int_0^y M(y')\mathrm{d}y' \,. \tag{4.12}$$

Using a top-hat function for $M(y)$, the meridional velocity is given by

$$v = \begin{cases} -\frac{1}{\rho\sigma} y \partial_z \rho w & \text{for } |y| \le Y_m \\ -\frac{1}{\rho\sigma}(Y_h - y)\partial_z \rho w & \text{for } Y_m < |y| < Y_h \\ 0 & \text{else} \end{cases} , \tag{4.13}$$

where we have used the boundary condition $v = 0$ at $y = 0, \pm Y_h$, which implies no mass flux across the boundaries. Contours of the meridional velocities are shown in Fig. 4.4

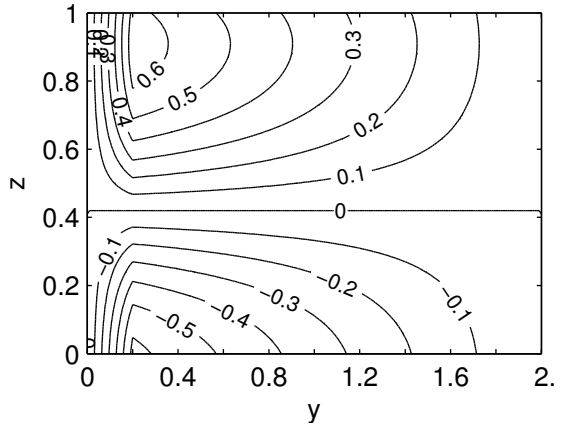

Figure 4.4: The meridional velocities for $Y_m = .2$

Above a critical height $z_c \sim 0.4$ ($\partial_z \rho w = 0$ at $z = z_c$) the flow is poleward and beneath it – equatorward. At the latitude $y = Y_m$ at the surface is located the minimum and in the upper

atmosphere the maximum of v. The magnitude of the extrema is proportional to Y_m (see (4.13)). Such distribution of meridional velocity is similar to observational profiles (Fig. 1.5).

4.2 The zonal wind

Taking into account that there is circulation only along stream lines with $\psi = const$, we can express the partial derivatives in the zonal momentum equation (2.59) as a directional derivative along such lines. If we use for example y to parameterize the stream lines:$\psi = \psi(z(y), y)$, then we have

$$\partial_y u + \underbrace{\frac{w}{v}}_{\frac{dz}{dy}} \partial_z u = \beta y + \frac{S_\alpha}{v} \,. \tag{4.14}$$

Or rewriting it in terms of a directional derivative along $\psi = const$ [1]

$$\frac{du}{dy}\Big|_{\psi=const} = \beta y + \frac{S_\alpha}{v} \,. \tag{4.16}$$

The new form of the zonal momentum equation can be easily integrated in the inviscid case

$$u = \frac{1}{2}\beta y^2 + C \,, \tag{4.17}$$

where C is an arbitrary constant for each stream line. In order to obtain an unambiguous solution for the zonal wind we have to give either a vertical profile of u for a particular latitude or a meridional profile for a constant height and determine from it C. In Section 4.4 we introduce the absolute zonal momentum $p_x = u - \frac{1}{2}\beta y^2$ and show that at the equator it cannot exceed zero in the presence of viscosity. This gives us a physical constraint: $C \leq 0$.

A unique solution can be found for the special case when we consider the flow at the top of the Hadley cell with $w = 0$. Then (2.59) can be integrated and implying the physical boundary condition $u = 0$ at the equator, we get

$$u(y, z = 1) = \frac{1}{2}\beta y^2 \,. \tag{4.18}$$

Thus in the inviscid case the zonal wind will grow quadratic, reaching its maximum at the edge of the Hadley cell.

[1] where we have the constraint:

$$\frac{dz}{dy} = \frac{w}{y} \tag{4.15}$$

From the integration of this equation follows that a particular function remains constant along stream lines, this is the stream function ψ.

Now we consider the viscous case with $S_u = -\alpha u$, using a Rayleigh representation of the source term (see Chapter 3). For simplicity we will look for solutions for $y \geq 0$ – the solutions for the northern and southern hemisphere are symmetric if the source term S_θ is symmetric about the equator. Its meridional and vertical distribution are given by (3.10) and (3.11), respectively.

Again we can represent (2.59) in terms of a directional derivative. But because v cannot be expressed as a function of y only, we have to do with transcendental equation for the particular choice of ρ and $Z(z)$, we select z as a parameter for representing $\psi(y(z), z)$ and obtain

$$\partial_z u + \underbrace{\frac{v}{w}}_{\frac{dy}{dz}} \partial_y u = \frac{du}{dz}\Big|_{\psi=const} = \beta y \frac{v}{w} - \frac{\alpha}{w} u \tag{4.19}$$

Integrating the homogeneous version of (4.19) for $0 \leq y(z) \leq Y_m$ yields

$$u_{l,h}(z) = C_l \tan^{-\frac{\alpha}{\pi}}(\frac{\pi z}{2}) \tag{4.20}$$

Using an ansatz $u_l = a(z) u_{l,h}(z)$ we obtain the solution for $0 \leq y(z) \leq Y_m$

$$u_l(z) = -\tan^{-\frac{\alpha}{\pi}}(\frac{\pi z}{2}) \int_{z_0}^{z} \beta \psi^2 \frac{\partial_z \rho w}{(\rho w)^3} \tan^{\frac{\alpha}{\pi}}(\frac{\pi z'}{2}) \mathrm{d}z + C_l \tan^{-\frac{\alpha}{\pi}}(\frac{\pi z}{2}) \tag{4.21}$$

With the same technique we get the solution for $Y_m \leq y(z) \leq Y_h$

$$u_r(z) = \tan^{\frac{\alpha}{\pi}}(\frac{\pi z}{2}) \int_{z_0}^{z} \beta \psi \left(Y_h - \frac{\psi}{\rho w} \right) \frac{\partial_z \rho w}{(\rho w)^2} \tan^{-\frac{\alpha}{\pi}}(\frac{\pi z'}{2}) \mathrm{d}z + C_r \tan^{\frac{\alpha}{\pi}}(\frac{\pi z}{2}) \tag{4.22}$$

Requiring continuity of u, we have $u_l \stackrel{!}{=} u_r$ at $y = Y_m$ and we can eliminate one arbitrary constant C_r

$$C_r = C_l \tan^{-\frac{2\alpha}{\pi}}(\frac{\pi z_0}{2}) \tag{4.23}$$

So the solution of the zonal wind consists of u_l for $0 \leq y \leq Y_m$ and u_r for $Y_m \leq y \leq Y_h$ and has the arbitrary constant $C_l := C$.

This constant can be found if we integrate (4.19) over a closed contour $\psi(y(z), z) = const.$

$$\oint_\psi \frac{du}{dz} \mathrm{d}z = \oint_\psi \beta y \frac{v}{w} \mathrm{d}z - \oint_\psi \frac{\alpha}{w} u \mathrm{d}z \tag{4.24}$$

The l.h.s. disappears, the contribution from the first integral on the r.h.s. is also zero. This is easily seen if you suppose $\alpha = 0$ (the inviscid case), or if you split the integration from z_0 to z_1 and from z_1 to z_0 (z_0, z_1 denotes the lowest and the most upper height of the stream line, respectively) and substitute the expressions for v, w (the index l,r denotes this part of the function where $0 \leq y < Y_m$,$Y_m > y \geq Y_h$ respectively)

$$\begin{aligned}\oint_{\psi=const} \beta y \frac{v}{w} \mathrm{d}z &= \int_{z_0}^{z_1} \beta y \frac{v_l}{w_l} \mathrm{d}z + \int_{z_1}^{z_0} \beta y \frac{v_r}{w_r} \mathrm{d}z \\ &= -\int_{z_0}^{z_1} \beta \psi^2 \frac{\partial_z \rho w_l}{(\rho w_l)^3} \mathrm{d}z + \int_{z_1}^{z_0} \beta \left(Y_h - \frac{\psi}{\rho w_l} \right) \psi \frac{\partial_z \rho w_l}{(\rho w_l)^2} \mathrm{d}z \\ &= \int_{z_1}^{z_0} \beta Y_h \psi \frac{\partial_z \rho w_l}{(\rho w_l)^2} \mathrm{d}z = -\beta Y_h \psi \int_{z_1}^{z_0} \mathrm{d} \left(\frac{1}{\rho w_l} \right) = 0\end{aligned} \tag{4.25}$$

where we have considered the special case when $Y_m = Y_h/2$ then $w_l = -w_r$. Finally, it follows that the last integral on the right hand side of (4.24) must be zero, or again splitting the limits of integration yields

$$\oint_{\psi} \frac{\alpha}{w} u \mathrm{d}z = \int_{z_0}^{z_1} \frac{\alpha}{w_l} u_l \mathrm{d}z + \int_{z_1}^{z_0} \frac{\alpha}{w_r} u_r \mathrm{d}z = 0 \tag{4.26}$$

Substituting our expressions for u and w we can regard the above equation as constraint on the constant C. So we find

$$C = \frac{-\int_{z_0}^{z_1} \frac{\alpha}{w_l} \{u_{l,p}(z) + u_{r,p}(z)\} \mathrm{d}z}{\int_{z_0}^{z_1} \frac{\alpha}{w_l} \{\tan^{-\frac{\alpha}{\pi}}(\frac{\pi z}{2}) + \tan^{-\frac{2\alpha}{\pi}}(\frac{\pi z_0}{2}) \tan^{\frac{\alpha}{\pi}}(\frac{\pi z}{2})\} \mathrm{d}z} \tag{4.27}$$

Where $u_{lp}(z)$ and $u_{rp}(z)$ are defined as

$$u_{l,p}(z) = -\tan^{-\frac{\alpha}{\pi}}(\frac{\pi z}{2}) \int_{z_0}^{z} \beta \psi^2 \frac{\partial_z \rho w}{(\rho w)^3} \tan^{\frac{\alpha}{\pi}}(\frac{\pi z'}{2}) \mathrm{d}z \tag{4.28}$$

$$u_{r,p}(z) = \tan^{\frac{\alpha}{\pi}}(\frac{\pi z}{2}) \int_{z_0}^{z} \beta \left(Y_h - \frac{\psi}{\rho w} \right) \psi \frac{\partial_z \rho w}{(\rho w)^2} \tan^{\frac{-\alpha}{\pi}}(\frac{\pi z'}{2}) \mathrm{d}z \tag{4.29}$$

We can conclude that we need a source term S_u in order to have unambiguous solution for the zonal wind.

4.2.1 Zonal wind with zero vertical velocity

Now we consider a special case of (2.59) where the vertical velocity vanishes. Such is the case at the surface and at the top of the Hadley cell (where we have $w = 0$ as boundary condition). Under this assumption the zonal momentum balance takes the form of the corresponding equation in the shallow water system.

Using the condition $w = 0$ and substituting the expressions for the meridional velocity (4.13), one finds the solutions of (2.59) for $z = 0, 1$

$$u = \begin{cases} \dfrac{\beta y^2}{2-a} + C_l y^a & \text{for } y \leq Y_m \\ \dfrac{-\beta(Y_h - y)}{1+a}\dfrac{ay + y + Y_h}{2+a} + C_r(y - Y_h)^a & \text{for } Y_m < y < Y_h \end{cases} \tag{4.30}$$

Where C_r and C_l are constants from the integration and a is given through

$$a = \frac{\alpha\rho}{\partial_z \rho w} \qquad \text{at } z = 0, 1 \tag{4.31}$$

The solution (4.30) fulfills automatically the boundary conditions $u(0) = u(Y_h) = 0$ even for $C_l, C_r \neq 0$. In Section 4.4 we discuss why it is physical meaningful to require a vanishing zonal wind at the equator. At the edge of the Hadley cell we can match u to a value of a geostrophically balanced wind from the midlatitudes, resulting from the meridional temperature gradient (the velocity can be computed using (4.37)). Without lost of generality the zonal wind can be set to zero at Y_h (Polvani and Sobel, 2002), this is used as a boundary condition for the numerical solutions in Chapter 5.

Suppose $a < 0$ in (4.30), this is the case at the top of the atmosphere where $v > 0$, then $\lim_{y\to 0} u = \infty$ which is not physical. We set $C_l = 0$ to go around this problem. Then C_r is found requiring continuity of u at Y_m. The solution for the zonal wind is sketched out in Fig. 4.5. As α increases, the maximum magnitude of the wind is reduced and it shifts toward the center of the cell. The same behavior was observed for large values of ν, see Section 5.3.1 for an explanation.

Analogously we find the solution for the lower branch of the circulation where $v < 0$ and thus $a > 0$. Then $\lim_{y\to Y_h} u = \infty$ and we set $C_r = 0$. The solution is presented in Fig. 4.6.

Note, the meridional profiles of u at $z = 1,\ 0$ are not symmetric (see (4.30)), even the maximum of the zonal wind at the surface is greater (although not significant) then this of the wind at the top of atmosphere, for the same α. As α decreases the magnitude of the easterlies increases. Such behavior of the surface wind is not observed in the numerical solution for u in the y, z-plane (see Section 5.3.2), due to the advection of air with nearly constant angular momentum. Here this effect is not included when we choose a boundary condition for (4.30) at $y = Y_h$, setting the wind to zero. Thus an air parcel at the edge of the cell has the zonal momentum of the earth (which is much smaller then the same at $y = 0$) and when transported equatorward it appears as strong easterly wind for $\alpha \to 0$.

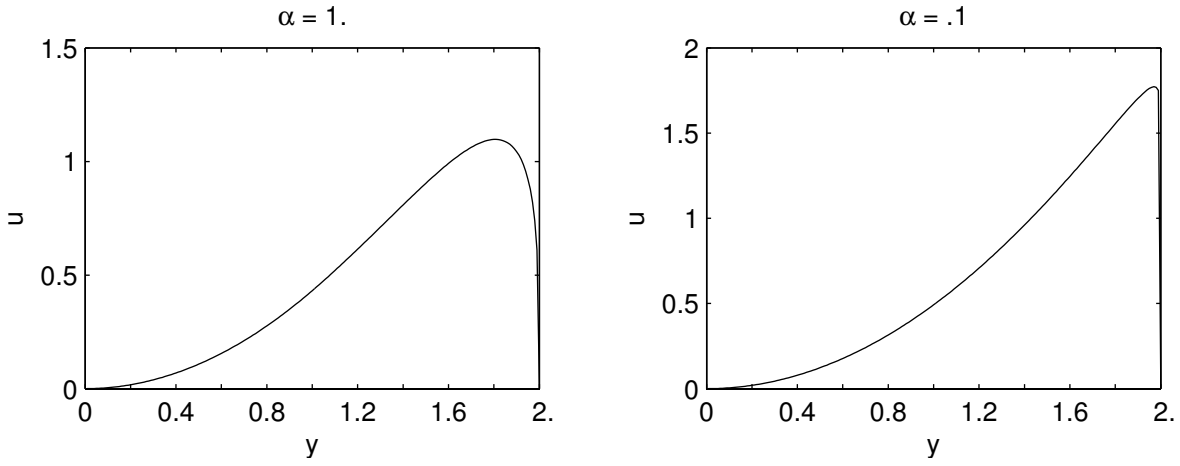

Figure 4.5: Zonal wind at $z = 1$ and for $Y_m = 1$.

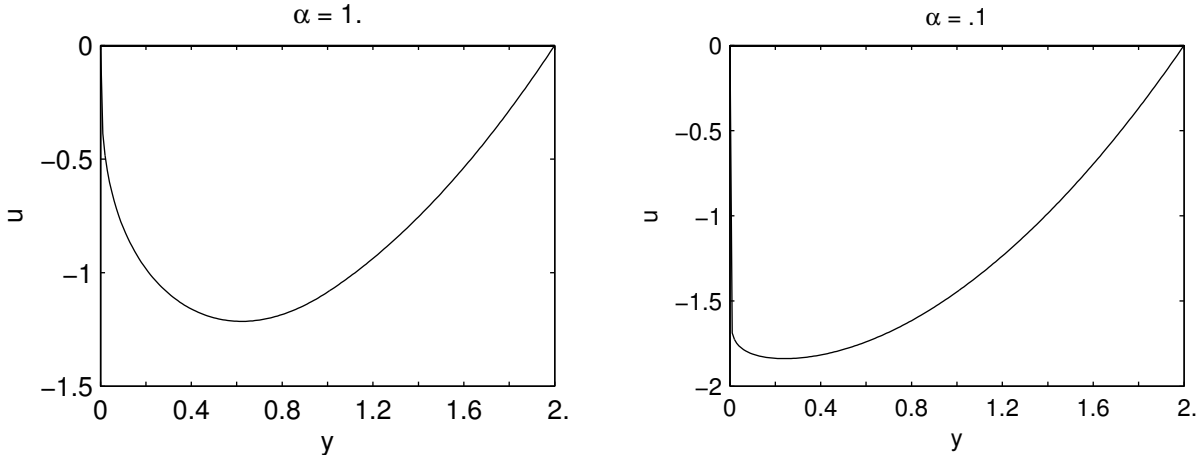

Figure 4.6: Zonal wind at $z = 0$ and for $Y_m = 1$.

4.3 Potential temperature distribution

We compute a meridional profile of the vertically integrated potential temperature $\theta^{(4)}$ using the meridional momentum balance (2.60) and the hydrostatic balance (2.36).

For simplicity we make the assumption that the source term $S_v = 0$, so we neglect the frictional effects. This is an appropriate approximation, if we consider the free atmosphere and if we are not interested on describing some boundary layer phenomena like the trade inversion. Then the zonal flow is in geostrophic balance, if the advection terms are sufficiently small. Some estimates of the advection terms will be made later on.

We differentiate (2.60) with respect to z and make use of the hydrostatic balance (2.36), thus obtaining the usual thermal wind relation with additional advection terms

$$\partial_z(v\partial_y v + w\partial_z v) + \partial_z \beta y u = -\partial_y \theta^{(4)} \tag{4.32}$$

Then we integrate over the whole depth of the atmosphere

$$v\partial_y v\Big|_{z=0}^{z=1} + w\partial_z v\Big|_{z=0}^{z=1} + \beta yu\Big|_{z=0}^{z=1} = -\partial_y \overline{\theta^{(4)}} \tag{4.33}$$

Where $\overline{\theta^{(4)}}$ denotes the vertically integrated potential temperature. Substituting our solution for the zonal wind in the inviscid case (4.18), and applying the physical boundary conditions $v = w = u = 0$ at $z = 0$ and $w = 0$ at $z = 1$ yields

$$v\partial_y v\Big|_{z=1} + \frac{1}{2}\beta^2 y^3 = -\partial_y \overline{\theta^{(4)}} \tag{4.34}$$

The integral over y of the above equation gives an expression for the distribution of $\overline{\theta^{(4)}}$

$$\overline{\theta^{(4)}(y)} = \begin{cases} -\frac{1}{8}\beta^2 y^4 - \frac{1}{2}v^2(y, z=1) + \theta_l & \text{for } y \leq Y_m \\ \\ -\frac{1}{8}\beta^2 (y^4 - Y_h^4) - \frac{1}{2}v^2(y, z=1) + \theta_r & \text{for } Y_m < y < Y_h \end{cases} \tag{4.35}$$

Where θ_l, θ_r are arbitrary constants. One constant can be found, requiring continuity of $\overline{\theta^{(4)}}$ at $y = Y_m$.

$$\theta_r = \theta_l - \frac{1}{8}\beta^2 Y_m^4 \tag{4.36}$$

The constant θ_l can be then interpreted as a contribution to the horizontally uniform mean potential temperature.

Fig. 4.7 represents the meridional distribution of $\overline{\theta^{(4)}}$ with and without the advection term in (4.34).

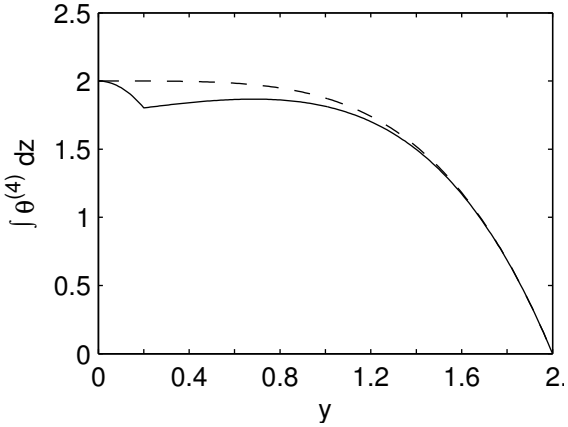

Figure 4.7: $\overline{\theta^{(4)}}$ with $\theta_l = 0$, dashed line solution without advection term

Large meridional temperature gradients occur near the edge of the Hadley cell. The reason for it one will find in the presence of the jet stream in the upper atmosphere at this latitudes, see Fig. 5.3. The zonal wind is nearly geostrophically balanced and because of the thermal wind

relation this implies a strong meridional temperature difference. Such drop of the temperature at the edge of the Hadley cell can be observed in the mean zonally averaged temperature distribution (Fig 1.6). Except in the area near the right boundary of the domain, $\overline{\theta^{(4)}}$ exhibits no large fluctuations. This agrees well with observations and is another justification of the assumption that in the tropics there are no large temperature fluctuations. However in the context of the derivation in Chapter 2 we must say that the constant background pressure stratification given by $\Theta_2(z)$ brings the WTG approximation of the energy equation. Here we observe that higher order corrections, represented by $\theta^{(4)}$, show homogeneity in particular regions.

The effect of the vertically averaged advection on the potential temperature can also be seen in Fig. 4.7 (solid curve). It does not change significantly the meridional distribution of $\overline{\theta^{(4)}}$. The baroclinity, associated with the kink at $y = 0.2$, can be explained through the maximum of v at this latitude in the upper atmosphere (Fig. 4.4). Because of the advection term in (4.34), $\overline{\theta^{(4)}}$ decreases for $y < 0.2$ and an increase for $y > 0.2$.

The meridional gradient of $\overline{\theta^{(4)}}$, computed from the numerical simulations, is presented in Fig. 4.8 (solid line). It is compared with the analytical solution (dashed line) for the inviscid case (4.34). In the region $y < 1$ there is no significant difference between the two curves (for $y < 0.2$ the two curves overlap) and the inviscid solution is a good approximation to the case with small friction. The discontinuity of the curves at $y = 0.2$ is due to the kink of $\overline{\theta^{(4)}}$ at this latitude. The local minimum of the solid curve at $y = 1.8$ corresponds to the position of the jet in the viscous case (the zonal wind is presented in Fig. 5.3 for $Y_m = 0.1$, here we used $Y_m = 0.2$). Its magnitude is reduced and this is evident from the discrepancy of the two graphs at this latitude. The imposed rigid wall at $y = 2$ in the case with friction is responsible for the increase of the slope of $\overline{\theta^{(4)}}$ near the edge of the Hadley cell.

From Fig. 4.8 we can also estimate how the geostrophic balance is affected by the nonlinear advection term. For the particular choice of parameters ($Y_m = 0.2$) the maximum magnitude of the advection term is ~ 2 at Y_m. It has to be balanced by a strong pressure gradient force (the zonal winds are weak at this latitude). For a latitude greater then 0.2 the advection term is much smaller. This is duo to the fact that the term $\partial_y v$ is proportional to H_e for $y < Y_m$ and to H_0 for $y > Y_m$, where $H_e \gg H_0$. We can conclude that the nonlinear advection term is particularly important in the heating region, especially when it is centered near the equator. Its maximum strength depends strongly on the magnitude of the potential temperature source term and the area of heating (the meridional integral in (4.12)). At higher latitudes the contribution from the advection term is negligible and the flow is geostrophically balanced.

4.4 Hide's theorem for a β-plane fluid

Hide's theorem (Schneider and Lindzen, 1977) characterizes the distribution of the total angular momentum for a viscous fluid on a rotating sphere. It states that the total angular momentum can reaches its maximum only at the surface and there can be no surface westerlies at the equator. The theorem incorporates conservation of angular momentum and has been used to verify simulations of the Hadley cell. Here we derive the analogy of the Hide's theorem for a fluid on rotating β-plane. This will help us to choose appropriate boundary conditions for our set of equations.

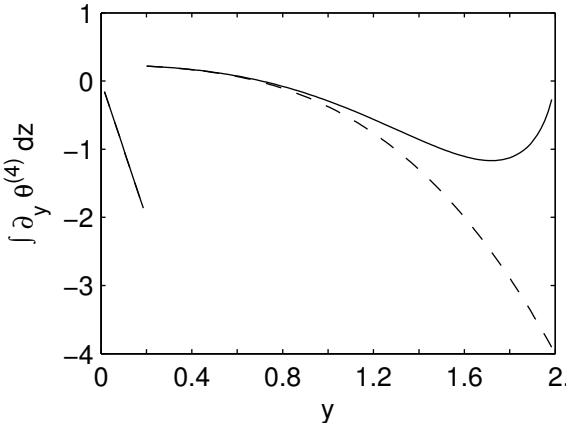

Figure 4.8: $\partial_y \overline{\theta^{(4)}}$ with $Y_m = 0.2$: dashed line inviscid solution, solid line with $\nu = 0.1$

Obviously $v = 0$ and $w = 0$ is a solution of our system of equations (2.59)-(2.62). Take into account the footnote at p. 12 for the following discussion. In the absence of frictional forces $S_u = S_v = 0$ we have a geostrophic balance for the zonal velocity, or from (4.33)

$$u(y, z = 1) = -\frac{1}{\beta y}\partial_y \overline{\theta}\,, \tag{4.37}$$

where $\overline{\theta}$ denotes the vertical average of the potential temperature and $\partial_y \overline{\theta} < 0$ (equilibrium temperature decreases poleward). If we assume that the meridional temperature gradient is nearly constant then the zonal wind will decline as $1/y$ and it will be everywhere westerly with a maximum at the equator. But such motion is not observed in the tropical atmosphere because of the presence of viscosity.

We can rewrite the equation for the zonal momentum balance (2.59) as

$$v\partial_y(u - \frac{1}{2}\beta y^2) + w\partial_z(u - \frac{1}{2}\beta y^2) = S_u\,, \tag{4.38}$$

or as

$$\boldsymbol{v} \cdot \nabla' p_x = S_u\,, \tag{4.39}$$

where $\nabla' = \boldsymbol{j}\partial_y + \boldsymbol{k}\partial_z$ and

$$p_x = u - \frac{1}{2}\beta y^2\,. \tag{4.40}$$

p_x can be interpreted as the x component of the total momentum per unit mass. It has contributions from the relative velocity of a parcel air and the earth's rotation velocity. Combining (4.39) with the continuity equation (2.61) we obtain:

$$\nabla' \cdot (p_x \rho \boldsymbol{v}) = \rho S_u\,, \tag{4.41}$$

which express only that the flux of zonal momentum is equal to the contribution of the sources. The source term in the zonal momentum balance equation can be represented (see Chapter 3) as

$$S_u = \frac{1}{\rho}\partial_z \mu \partial_z u \,, \tag{4.42}$$

where μ is the eddy viscosity coefficient. For simplicity we assume $\mu = const$, (4.41) takes the form:

$$\nabla' \cdot (p_x \rho \boldsymbol{v}) = \mu \partial_{zz} p_x \,. \tag{4.43}$$

Suppose that p_x has a maximum within the fluid and that it is continuous in space. Then we can always find a closed contour $\delta\Omega$ around this maximum where $p_x = const$. Integrating (4.43) over the area closed by this contour, it follows:

$$p_x \oint\limits_{\delta\Omega} \boldsymbol{n} \cdot \rho \boldsymbol{v} \mathrm{d}s = \int\limits_{\Omega} \mu \partial_{zz} p_x \mathrm{d}f \,. \tag{4.44}$$

We have used the $2D$ Gauss theorem and $\boldsymbol{n}$ denotes the vector normal to $\delta\Omega$. The integral on the l.h.s. vanishes because of the continuity equation (2.61). The contribution of the r.h.s. will be negative: p_x has its maximum in Ω so $\partial_{zz} p_x < 0$, down gradient fluxes of p_x will occur along $\delta\Omega$. This contradiction implies that p_x cannot reach its maximum in the interior of the fluid. Similar arguments are applied if we assume that p_x has a maximum on a stress-free boundary (the tropopause in our model). Now suppose p_x has a maximum at the lowest level of the atmosphere z_0. Then we can draw a contour of constant p_x above the surface and close it along the surface. The integral on the l.h.s. of (4.44) is vanishing again due to mass conservation and $w = 0$ at the surface. The value of the integral over the source term depends on the direction of the winds at the surface. There is a thin layer between the surface at z_s and the level z_0 where the surface winds are measured, so $u(z_s) = 0$ but we can have $u(z_0) \neq 0$. If the surface winds are easterly we have a flux of p_x along the surface line into Ω. The flux is given through $-\nabla' p_x$ or at the surface as $\boldsymbol{n}\partial_z p_x$, where $\boldsymbol{n} = -\boldsymbol{k}$. Since $u(z_s) > u(z_0)$ it will be directed into Ω. Along the rest of $\delta\Omega$ the flux is directed outwards, because p_x maximal at z_0. Thus there is a possibility that both fluxes compensate, then the integral over Ω vanishes and (4.44) is fulfilled. This is not the case if the surface winds are westerly. Then along the surface the flux of p_x will be directed also outwards: $u(z_s) < u(z_0)$.

Thus p_x can have only maximum at the surface with $u \leq 0$. The maximum value is $p_x = 0$ at the equator with $u = 0$ at the surface. This condition implies conservation of zonal momentum and it is often used to check zonally symmetric models for physical consistency - it is violated when the model produces westerly winds over the equator. It rejects the proposed thermally balanced solution for the zonal wind (4.37). Later we will demand $u(z, y = 0) = 0$ at the equator as a boundary condition, and the discussion shows that this is a reasonable assumption. In this case we suppose that the rising air from the surface conserves the maximum zonal momentum.

Chapter 5

Numerical Solution

The zonal momentum balance equation was solved numerically using a vertical eddy diffusion source term S_u. In this chapter we present the numerical method, discuss the obtained solutions and compare them with the analytical solutions from Chapter 4.

5.1 Upwind discretization

The first idea was to divide (2.59) by v and to consider the derivative with respect to y as a "time" derivative. Then the zonal momentum balance equation takes the form of a parabolic equation. Having the "initial" conditions $u(y = 0, z) = 0$ and Dirichlet boundary condition at the bottom: $u(y, z = 0) = 0$ and von Neumann at the top $\partial_z u = 0$ at $z = 1$ we have an initial value problem. A standard approach for this type of equations is to use a forward difference scheme for the time derivative (y derivative in our case) and a central differences for the advection term and for the diffusion term. But as Morton and Mayers (1994) pointed out, this scheme requires enormous number of mesh points, when the advection therm is not negligible, in order to be stable. As a matter of fact we could achieve stability with this approach only when the advection term $w/v\partial_z u$ was set to zero (it tends to infinity as $v \to 0$). In this case the equation reduces to a diffusion equation in one space direction.

The problem with stability can be avoided if we do not modify (2.59) and use a upwind discretization for the advection terms (Morton and Mayers, 1994). It is a standard discretization for the advection in a hyperbolic equation (Press et al., 2002). Another advantage of this scheme is when the transport of a tracer is considered. This discretization takes into account the sign of the wind, so a disturbance can be spread only in the direction of the wind.

We define a discrete domain Ω with $P,\ M$ points in y and z direction respectively:

$$\Omega = \{(y_i, z_j) : y_i = i\Delta_y, z_j = j\Delta_z, 1 \leq i \leq P, 1 \leq j \leq M\} \tag{5.1}$$

Where $\Delta_y = Y_h/(P-1)$ and $\Delta_z = 1/(M-1)$. Then a function $u(y, z)$ can be represented on the discrete set of points as

$$u(y,z) = u(i\Delta_y, j\Delta_z) = u_{i,j} \tag{5.2}$$

Using the upwind discretization, the advection term in the direction of v takes the form:

$$v\partial_y u \text{ at (i,j)} = \begin{cases} \dfrac{v_{i,j}}{\Delta y}(u_{i,j} - u_{i-1,j}) & : \text{if } v_{i,j} > 0 \\ \\ \dfrac{v_{i,j}}{\Delta y}(u_{i+1,j} - u_{i,j}) & : \text{if } v_{i,j} < 0 \end{cases} + \mathcal{O}(\Delta y) \tag{5.3}$$

Upwind discretization is also used for the $w\partial_z u$ term. Because v and w change sign in the domain of interest we have to distinguish altogether four different cases when applying this scheme for equation (2.59).

For the diffusion term $1/\rho\partial_z\mu\partial_z u$ a central difference scheme is utilized, where $\nu = \mu/\rho$ is computed on a staggered grid

$$\begin{aligned} \frac{1}{\rho}\partial_z\mu\partial_z u \text{ at (i,j)} &:= \frac{1}{\rho_{i,j}}\frac{1}{\Delta z^2}\left(\mu_{j+1/2}(u_{i,j+1} - u_{i,j}) - \mu_{j-1/2}(u_{i,j} - u_{i,j-1})\right) + \mathcal{O}\left(\Delta z^2\right) \\ &= \frac{1}{\Delta z^2}\Big(\underbrace{\frac{\mu_{j+1/2}}{\rho_{i,j+1/2}}}_{\nu_{i,j+1/2}}(u_{i,j+1} - u_{i,j}) - \underbrace{\frac{\mu_{j-1/2}}{\rho_{i,j-1/2}}}_{\nu_{i,j-1/2}}(u_{i,j} - u_{i,j-1})\Big) + \mathcal{O}\left(\frac{\Delta z}{2}\right) \end{aligned} \tag{5.4}$$

As boundary condition we use vanishing zonal velocity at the bottom $u(y, z = 0) = 0$ and no stress condition at the top $\partial_z u(y) = 0$ at $z = 1$.

For the $v\partial_y u$ term we need a boundary condition at $y = 0$ for $v > 0$. We will set $u = 0$ at this boundary, implementing the condition of maximum absolute zonal momentum at the equator, see Section 4.4. For the case of $v < 0$ at $y = Y_h$ a physical boundary condition can be obtained if we assume that outside the Hadley cell the zonal wind is geostrophically balanced $\beta y u_g = -\partial_y \pi^{(4)}$ for $y > Y_h$ and match u to u_g at Y_h. In this case we must prescribe a meridional pressure gradient which will result from a meridional radiative equilibrium temperature gradient. But since we are interested on dynamics driven by convection for simplicity we will set this gradient outside the cell to zero thus obtaining $u_g = 0$ for $y > Y_h$. So we have a rigid boundary for the Hadley cell at $y = Y_h$ with $u(Y_h, z) = 0$.

Substituting the described above finite-difference representations for the differential operators in (2.59) and implementing the boundary conditions we obtain a system of $P * M$ linear equations . This system is written in matrix form

$$\mathbf{A}\mathbf{u} = \mathbf{b} \tag{5.5}$$

Where $\mathbf{A}$ is constructed from the discrete differential operators and is called "tridiagonal matrix with fringes". The structure of this sparse matrix is displayed in Fig. 5.1. The vector $\mathbf{u}$ is made up of the values of $u_{i,j}$ on the grid and $\mathbf{b}$ is the inhomogeneity containing the terms $\beta y v_{i,j}$. The linear system is then solved for $\mathbf{u}$.

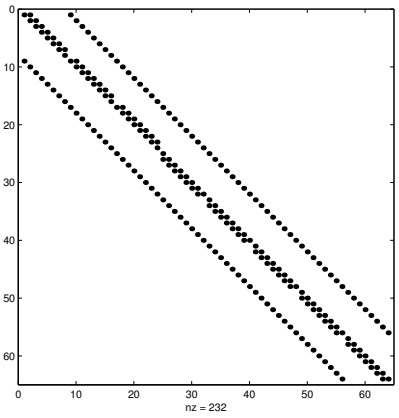

Figure 5.1: Non-zero arguments of the matrix $\mathbf{A}$ with 64×64 elements

5.2 Stability study and convergence order

In all performed simulations the numerical method remained stable, and the solution for the particular setup had a physically reasonable structure.

A stability study was made, running experiments with different number of grid points for the same setup. From the set of results a convergence order of one was estimated for the scheme. This is not surprising, since the lowest order discretization we have used is the upwind of order one (5.3).

The global error defined as a vector is:

$$\mathbf{e} = \mathbf{u} - \mathbf{u_a} \tag{5.6}$$

Where $\mathbf{u}$ is the discrete solution vector and the components of $\mathbf{u_a}$ are the exact analytical solution on the grid. Then for the order of accurate p of the method we have the following relation

$$E = \|\mathbf{e}\| = Ch^p + \mathcal{O}(h^p) \qquad \text{as } h \to 0 \tag{5.7}$$

Where we choose an appropriate norm, h denotes the grid spacing on a uniform grid and C is a constant. Suppose we can compute the solution on three different grids with spacing: h_0, h_1, h_2 respectively and we have

$$h_2 = \frac{h_1}{2} = \frac{h_0}{4} \tag{5.8}$$

But since the analytical solution is not known we introduce the approximate error analogous to the global error

$$E_1 = \|\mathbf{u_1} - \mathbf{u_2}\| \qquad E_0 = \|\mathbf{u_0} - \mathbf{u_1}\| \tag{5.9}$$

Where the index of $\mathbf{u_i}$ denotes the grid on which the solution was computed ($i = 1$ corresponds to the grid h_1 and so on). In order tho calculate the difference between $\mathbf{u_i}$ and $\mathbf{u_{i+1}}$ we take only this values of the vectors which coincide with values of $\mathbf{u_0}$ on the coarsest grid h_0. Then we can make the following estimate for the error E_1, making use of (5.7)

$$\begin{aligned} E_1 &= \|(\mathbf{u_1} - \mathbf{u_a}) - (\mathbf{u_2} - \mathbf{u_a})\| \\ &\leq \|(\mathbf{u_1} - \mathbf{u_a})\| + \|(\mathbf{u_2} - \mathbf{u_a})\| \\ &\approx Ch_1^p + Ch_2^p \end{aligned} \tag{5.10}$$

Similarly

$$E_0 \approx Ch_0^p + Ch_1^p \tag{5.11}$$

If we build the ratio of the approximate errors, substituting (5.7) we get

$$\rho = \frac{E_1}{E_0} = \frac{h_1^p}{h_0^p} \frac{1 + \dfrac{1}{2^p}}{1 + \dfrac{1}{2^p}} = \frac{1}{2^p} \tag{5.12}$$

Then the convergence order is given through

$$p = \frac{\ln \rho}{-\ln 2} \tag{5.13}$$

This result can be easily extended from three to n sets of solutions. Then we can compute $n - 2$ error ratios and convergence orders

$$\rho_{i-1} = \frac{\|\mathbf{u_{i+1}} - \mathbf{u_i}\|}{\|\mathbf{u_i} - \mathbf{u_{i-1}}\|} \qquad p_{i-1} = -\frac{\ln \rho_i}{\ln 2} \qquad i = 2 \ldots n-1 \tag{5.14}$$

We have performed a number of experiments reducing the grid spacing by a factor of two after each simulation (uniformly spaced grid). The runs are summarized in Table 5.1.

simulation i:	1	2	3	4	5
grid points	32×32	64×64	128×128	256×256	512×512

Table 5.1: Notation of the experiments

The calculated convergence orders are presented for the $\|\cdot\|_1$ norm in Table 5.2, and for the $\|\cdot\|_2$ norm in Table 5.3. It is interesting to note that the second experiment shows a higher convergence order than the first. A reason for this can be that the 32×32 points we use to compute the matrix norms (for all simulations) are still not sufficient. Taking into account the results, we can conclude that for $\Delta z, \Delta y \to 0$ the numerical scheme converges to 1.

simulation	1	2	3
convergence order	1.0308	1.1084	1.0011

Table 5.2: Convergence order with the $\|\cdot\|_1$ norm

simulation	1	2	3
convergence order	1.0154	1.0449	1.0049

Table 5.3: Convergence order with the $\|\cdot\|_2$ norm

5.3 The zonal velocity u

A series of simulations has been performed for a prescribed top-hat S_θ: (3.9),(3.10) and (3.11). Two different parameterizations for the momentum source terms ware used, they ware discussed in detail in Section 3.3. Here we will present the solutions for the particular choice of parameters.

We have used as boundary conditions:

- Maximum zonal momentum at the equator (see Section 4.4)

$$u(y = 0, z) = 0 \tag{5.15}$$

- No-slip boundary condition at the surface

$$u(y, z = 0) = 0 \tag{5.16}$$

- Neglect of interactions with waves from the stratosphere - no-stress condition at the tropopause

$$\partial_z u = 0 \text{ at } z = 1 \tag{5.17}$$

- And a rigid wall at the edge of the cell (see the discussion of the boundary conditions in Section 4.2.1)

$$u(y = Y_h, z) = 0 \tag{5.18}$$

5.3.1 Vertical diffusion: $S_u = \frac{1}{\rho}\partial_z \mu \partial_z u$

The profile $\nu = \mu/\rho$ is displayed in Fig. 5.2, right plot. $\nu_b = 0.5$ represents the value of the eddy viscosity in the boundary layer $0 < z < 0.1$, and ν_f the same but in the free atmosphere $z > 0.2$.

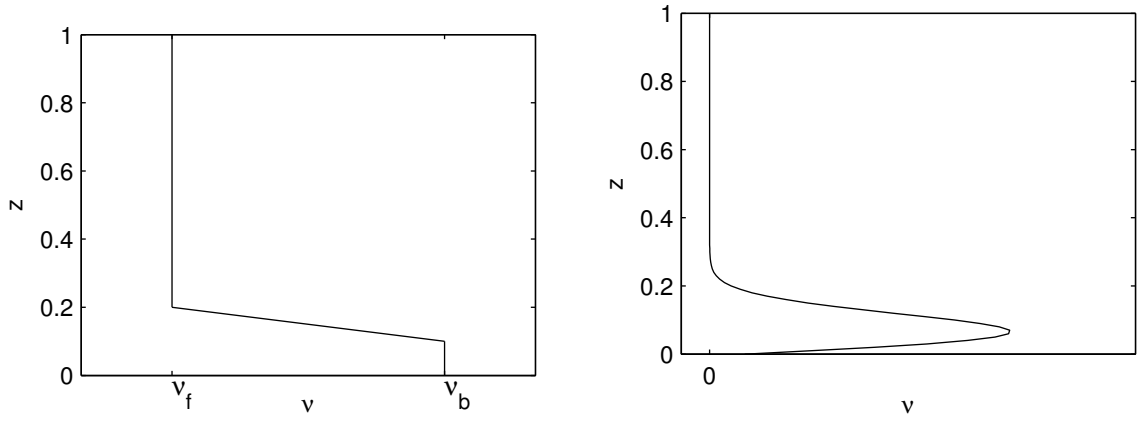

Figure 5.2: The ν-profile, linear and smooth

All simulations performed with different ν_f values have shown a westerly jet in the upper atmosphere (see Fig. 5.3). Its maximum is positioned at the tropopause, because of the no-stress boundary condition there, and its magnitude reduces as ν increases. As $\nu \to 0$ the core of the jet shifts to $y = Y_h$ but never reaches the edge of the cell, due to the rigid wall. For large ν the maximum of the jet is located at the center of the domain. This behavior can be understood, if we neglect the advection terms in (2.59). Then, we obtain an ODE for u

$$-\beta \rho y v = \partial_z \mu \partial_z u \,. \tag{5.19}$$

The y dependent part of the solution for the zonal velocity has a maxima at $y = Y_h/2$. In the free atmosphere $\nu \to 0$ and the westerly jet we observe near the edge of the Hadley cell corresponds to the subtropical jet (see Fig. 1.4).

The model can reproduce easterly winds near the equator. There is a dependence of the magnitude of the easterlies on the strength (H_e) and the region ($y \leq Y_m$) of the forcing. Fig. 5.4 represents the zonal wind with a larger heating region: $Y_m = 1$. If we compare the left plot with the corresponding plot in Fig. 5.3, a maximum of easterlies (~ -0.2) strikes. We give here an explanation for this observation. In the lower atmosphere, air with low values of absolute zonal momentum at high latitudes is pumped equatorward (meridional advection) and it appears as easterly winds. As the forcing increases, the meridional transport intensifies and is more effective than the dissipation processes. Thus the magnitude of the easterly winds also increases. The same mechanism is responsible for the higher magnitude of the westerly jet. We still have zero zonal velocities for all z right at the equator due to the maximum zonal momentum boundary condition.

Note that all winds at $z = 0$ are zero, because of the no-slip boundary condition. More realistic surface winds can be simulated if we use a surface drag boundary condition: $\mu \partial u = Cu$, where C is a drag coefficient. For more details see Section 1.4.

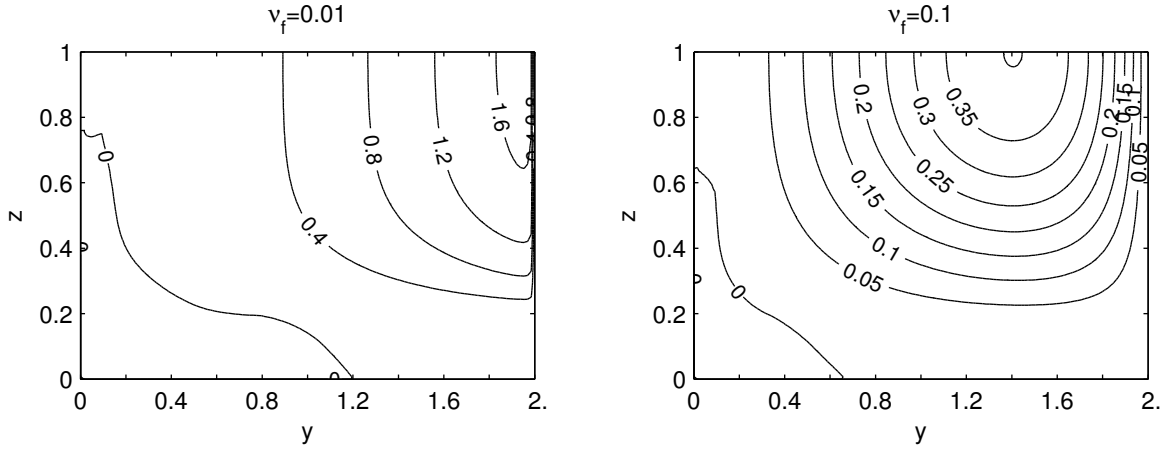

Figure 5.3: The zonal wind for $Y_m = 0.1$

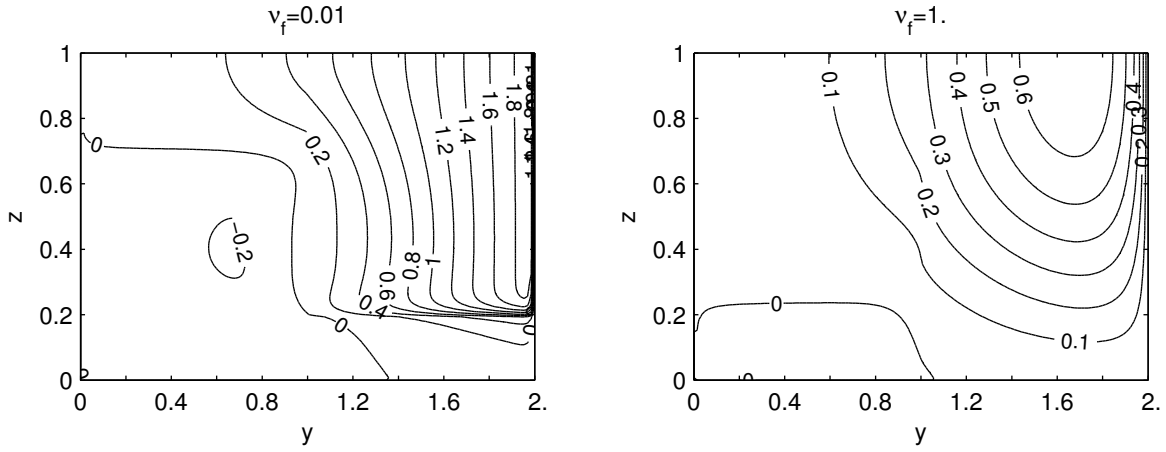

Figure 5.4: The zonal wind for $Y_m = 1$.

Experiments with a smooth ν-profile have been performed (see Fig. 5.2, right plot), taking into account the variations of the eddy viscosity within the boundary layer. We have varied the maximum of ν and its position. We could observe that, when the magnitude of the diffusion coefficient was reduced, the westerly jet was spread more deeper in the lower atmosphere. The increase of ν within the boundary does not affect significantly the zonal wind profile because of the small surface winds and the coarse resolution of the model.

We are interested on the westerly jet at $3500\,\text{km}$ ($\sim 30^\circ N$), see Fig. 5.5. The maximum value of the velocity is $\sim 120\,\text{m s}^{-1}$. This magnitude agrees well with more sophisticated models of the Hadley cell (Schneider and Lindzen, 1977; Schneider, 1977; Held and Hou, 1980; Lindzen and Hou, 1988). But a feature of all these models is that they overestimate the zonal wind, see Fig. 1.4. The reason for this is the neglect of horizontal eddies. In the presence of such strong jet barotropic and baroclinic eddies will obviously appear and reduce its magnitude.

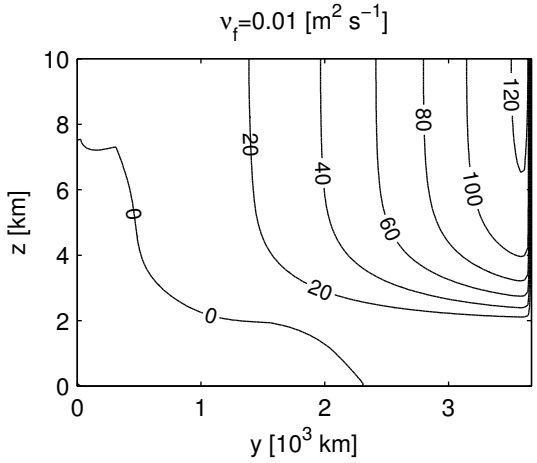

Figure 5.5: The zonal wind $[m\ s^{-1}]$

5.3.2 Relaxation parameterization: $S_u = -\alpha u$

Experiments were performed with a Rayleigh parameterization of the source term. The results are displayed in Fig. 5.6. The westerly and the easterly jet in the left plot can be explained as a result of meridional advection again. The vertical advection causes that for $y \leq Y_m$ (w is maximal in this region) and $\alpha = 0.5$ the 0.2 contour of the easterly jet is spread through the hole depth of the atmosphere. The closed contours of the jet at the surface and the opened at the top of the domain are due to the no-slip and no-stress boundary conditions there, respectively. As $\alpha \to 0$ the magnitude of the westerly jet increases ($u \to 1/2\beta Y_h^2$) but this of the easterly jet decreases. This can be explained in the following way: the air parcels nearly conserve their absolute angular momentum and they reach the equator with the maximal possible value: $p_x = 0$ for $u = 0$ (see Section 4.4), so no surface easterlies are observed. For $\alpha \to 0$ the solution for u approaches the inviscid solution (4.17), with $C = 0$ for all stream lines. The same behavior of the zonal wind can be observed for $\nu \to 0$. Experiments were also performed with $\alpha = 0$ and $\nu = 0$ and the distribution of u was very similar to the right plot in Fig 5.6. The imposed no-slip condition at the surface and the rigid wall at the edge of the cell modify the zonal wind at the boundaries from the inviscid solution (4.17).

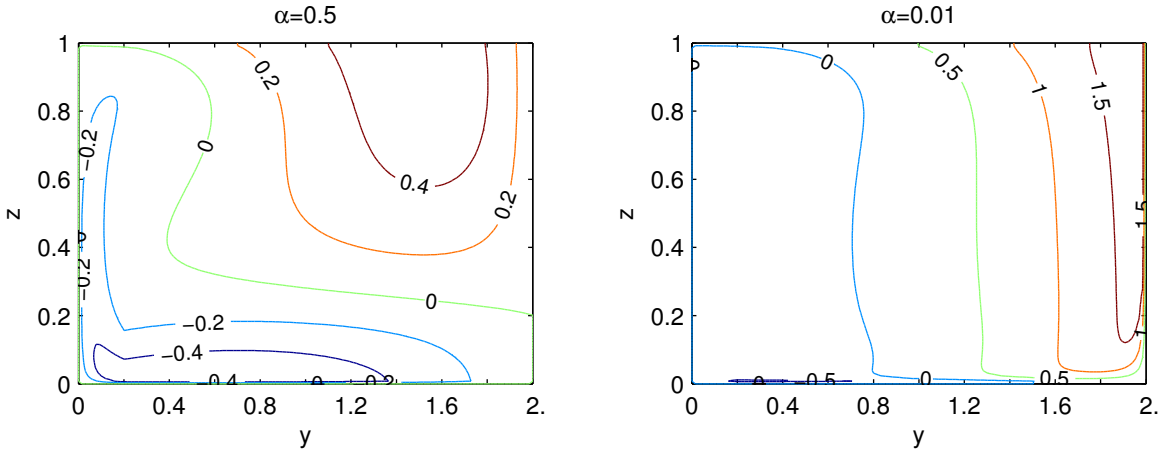

Figure 5.6: The Zonal wind for $Y_m = 0.1$

Summary

In order to investigate the atmospheric dynamics in the tropics, we applied an unified multiple scales asymptotic approach (Klein, 2000, 2004). An universal small parameter ε was introduced and the characteristic numbers in the governing equations were expressed in terms of it in a carefully chosen distinguished limit. This systematic approach was applied to the 3D compressible equations for a fluid on an equatorial β-plane. The same anisotropic asymptotic scaling as this proposed in Majda and Klein (2003) for their seasonal sub-planetary equatorial weak temperature gradient (SPEWTG) regime was used. Here we consider the case when a stronger potential temperature source term, representing convective processes, is allowed. This has as an effect that the meridional and vertical velocities are an order of magnitude larger then this in the SPEWTG regime. New steady-state reduced model equations were derived, they describe a flow on a sub-planetary length scale in zonal direction and a mesoscale in meridional direction. They include the WTG approximation and a nondivergent constraint on the flow in the y, z-plane. The momentum equations have important nonlinear transport terms.

It is a model of a Hadley type circulation modified by a zonal pressure gradient force. After consideration of the magnitude of the different diabatic processes, we showed that convective heating will drive the circulation. Due to energy conservation the latent heat release have to be balanced by radiative cooling, which is one order of magnitude smaller. In order to lighten the discussion of this system of equations, we applied a simple parameterization of the diabatic source term by prescribing its variations. For this purpose a top-hat function was used, where the positive part represents the convective heating centered at the equator. It is a model of the narrow band of the ITCZ, the zone with the most precipitation in the tropics. For the vertical profile of the upper level heating a sinusoidal distribution was assumed. It is in accordance with the observations of convecting ensembles, where the highest vertical velocities and thus the largest condensation rates appear in the divergence-free level.

Analytical solutions for the vertical and the meridional velocities were found. There are ascending motions in the region of heating and descending in the region of cooling, consistent with the WTG approximation. The magnitude of the vertical speed is close to the observed: $4\,\mathrm{cm\ s^{-1}}$ in the area of large-scale convection and $0.4\,\mathrm{cm\ s^{-1}}$ in non-precipitating area. The meridional velocities match to an ideal Hadley cell – poleward flow in the upper atmosphere and equatorward in the lower atmosphere. They show a minimum at the surface and a maximum in the upper atmosphere at the latitude of the cell center (where there are no vertical velocities), which is consistent with observations. It is important to mention that the region of ascent in our model is much smaller than that of descent, due to the different strength of the convective and the radiative processes. Seasonal averaged observations indicate the presence of a more or less symmetric winter Hadley cell. The reason for this is the ITCZ: it changes its position over

large area in this period and thus makes the region of heating comparable with this of cooling on average. In this case we could simulate a symmetric cell also.

To find solutions for the zonal wind we considered the zonally averaged version of the x-component of the momentum equation. In the inviscid case we showed that the absolute zonal momentum per unit mass $p_x = u - 1/2\beta y^2$ remains constant along stream lines. The solution of the zonal wind is unique only when friction is included. In the case of a Rayleigh parameterization of the momentum sink, the solution of the PDE was reduced to the calculation of integrals. Analytical solutions for u at $z = 1, 0$ were found. At the surface easterlies were predicted. We discussed the unrealistic increase of their magnitude as the friction tends to zero. At the top of the atmosphere a westerly jet was observed. Numerical simulations were performed with vertical diffusion, representing turbulent momentum transport. An upwind discretization for the advection terms and a central difference scheme for the diffusion term were applied. The numerical method was tested for stability and convergence. A strong upper level westerly jet near the edge of the Hadley cell was simulated. It has a magnitude of $120\,\mathrm{m\,s^{-1}}$ at $30^\circ N$ and corresponds to the subtropical jet. The high value of the maximum wind speed is not realistic because of the neglect of horizontal eddies. The reason for the westerly jet is that in the upper atmosphere the zonal momentum remains nearly conserved. The earth's rotation velocity decreases at higher latitudes, so an air parcel moving poleward has to increase its relative velocity. The same mechanism is responsible for the surface easterlies we simulated near the equator. Because of friction their magnitude is strongly reduced. The shift of the westerly jet to the center of the domain for large values of the friction was explained. In the inviscid case the numerical solution tends to the analytical solution for $\alpha = 0$ at $z = 1$, although boundary effects are visible.

Some estimates of the magnitude of the advection terms were made. They are important near the equator and in the heating region, at the higher latitudes the flow is geostrophically balanced. The distribution of the vertically integrated potential temperature is consistent with the wind field. It is homogeneous over large area in accordance with the WTG approximation and shows strong baroclinity at the position of the jet.

In order to study the interactions between a convective system and the lage-scale flow, a moisture budget has to be included. The moist static energy can be calculated, it determines the arise and the development of convection. It remains the question what parameterization of convection to apply. We have discussed a Kuo-type scheme, regarding the convective heating as an "external" source. Another approach, implemented in the quasi-equilibrium (QE) parameterization, is to put a constraint on the lage-scale flow in a convecting atmosphere. This is realized by prescribing an equilibrium profile (e.g. of the temperature) to which the convecting atmosphere tends to adjust. This profile can be modified e.g. by downdraughts and thus complex interactions can be included. The convection effects significantly the radiation budget in the tropics. The dependence of the longwave fluxes on temperature and moisture has to be taken into account. The cloud albedo has to be represented in the model, this leads to the question of stratus and cirrus parameterizations. If we are interested on atmosphere-land interactions some important properties of the continents have to be included – low-heat capacity, vegetation dependent albedo, different roughness, moisture sink. Representing the processes listed above, we will develop a model of intermediate complexity, able to reproduce realistic tropical circulation. Finally, we have to mention that through the asymptotic expansion we derived model equations which include a time dependence. Here we dealt with the steady-state version only, but we can

use this equations to address the challenging issue of the time evolution of the flow on the T_M time scale.

Acknowledgements

I want to thank Prof. Dr. Rupert Klein and PD Dr. Peter Névir for the supervision of my Diploma thesis. Furthermore, I want to thank Prof. Dr. R. Klein for giving me the chance to write my thesis at the Potsdam Institute for Climate Impact Research (PIK) and for the helpful guidance I received from him during my work.

In addition I especially want to thank Prof. Dr. Vladimir Petoukhov for his advises and Dr. Antony Owinoh for his help and for the proof-reading of the manuscript. I want to thank the whole group at PIK, especially Dr. Nicola Botta, Eileen Mikusky, Gunter Carqué and Stefan Vater for providing advice and a friendly atmosphere.

Finally, I want to say “thank you” to my family for their support and help over the last 24 years.

Bibliography

Arakawa, A. and Schubert, W. (1974). Interaction of a cumulus cloud ensemble with the large-scale environment, Part I. *J. Atmos. Sci.*, 31:674–701.

Betts, A. K. (1986). A new convective adjustment scheme. Part I: Observational and theoretical basis. *Quatr. J. Roy. Meteor. Soc*, 112:677–691.

Betts, A. K. and Miller, M. J. (1986). A new convective adjustment scheme. Part II: Single column tests using GATE wave, BOMEX, and arctic air-mass data sets. *Quatr. J. Roy. Meteor. Soc*, 112:993–709.

Bretherton, C. and Sobel, A. (2003). The Gill model and the weak temperature gradient approximation. *J. Atmos. Sci.*, 60:451–460.

Bretherton, C. S. and Sobel, A. H. (2002). A Simple Model of a Convectively Coupled Walker Circulation Using the Weak Temperature Gradient Approximation. *Journal of Climate*, 15:2907–2920.

Bronstein and Semendjajew (1993). *Taschenbuch der Mathematik*. Harry Deutsch, Frankfurt am Main.

Browning, G. L. and Kreiss, H.-O. (1997). The Role of Gravity Waves in Slowly Varying in Time Mesoscale Motions. *Journal of Atmospheric Sciences*, 54:1166–1184.

Browning, G. L., Kreiss, H.-O., and Schubert, W. H. (2000). The Role of Gravity Waves in Slowly Varying in Time Tropospheric Motions near the Equator. *Journal of Atmospheric Sciences*, 57:4008–4019.

Charney, J. and Eliassen, A. (1964). On the growth of hurricane depression. *J. Atmos. Sci.*, 21:68–74.

Charney, J. G. (1963). A Note on Large-Scale Motions in the Tropics. *Journal of Atmospheric Sciences*, 20:607–608.

Emanuel, K., Neelin, D., and Bretherton, C. (1994). On large-scale circulations in convecting atmospheres. *Quatr. J. Roy. Meteor. Soc*, 120:1111–1143.

Emanuel, K. A. (1994). *Atmospheric Convection*. Oxford University Press, New York.

Fang, M. and Kit Tung, K. (1999). Time-Dependent Nonlinear Hadley Circulation. *Journal of Atmospheric Sciences*, 56:1797–1807.

Gill, A. (1980). Some simple solutions of heat-induced tropical circulation. *Quatr. J. Roy. Meteor. Soc*, 106:447–462.

Gill, A. (2003). *Atmosphere-Ocean Dynamics*. Academic Press, New York.

Hansen, J., Russel, G., Rind, D., Stone, P., Lacis, A., Lebedeff, S., Ruedy, R., and Travis, L. (1983). Efficient three dimensional global models for climate studies: Models I and II. *Monthly Weather Review*, 111:609–662.

Heckley, W. A. and Gill, A, E. (1984). Some simple analytical solutions to the problem of forced equatorial long waves . *Quatr. J. Roy. Meteor. Soc*, 110:203–217.

Held, M. and Hou, A. (1980). Nonlinear axially symmetric circulation in a nearly inviscid limit. *J. Atmos. Sci.*, 37:515–548.

Holton, J. (1992). *An Introduction to Dynamic Meteorology*. Academic Press, New York.

Kamenkowitch (1973). *Basics of Ocean Dynamics*. Gidrometeoizdat. [In Russian].

Klein, R. (2000). Asymptotic analyses for atmospheric flows and the construction of asymptotically adaptive numerical methods. *Zeitschr. Angew. Math. Mech.*, 80:765–770.

Klein, R. (2004). An applied mathematical view of theoretical meteorology. In Hill, J. and Moore, R., editors, *Applied Mathematics Entering the 21st Century, invited talks at the ICIAM 2003 Conference*, volume 116 of *SIAM proceedings in Applied Mathematic*.

Kuo, H. L. (1974). Further Studies of the Parameterization of the Influence of Cumulus Convection on Large-Scale Flow. *Journal of Atmospheric Sciences*, 31:1232–1240.

Lange, H. J. (2002). *Die Physik des Wetters und des Klimas*. Reimer, 1 edition.

Lindzen, R. and Hou, M. (1988). Hadley circulation for zonally averaged heating centered off the equator. *J. Atmos. Sci.*, 45(17):2416–2427.

Lindzen, R. S. (1990). *Dynamics in Atmospheric Physics*. Cambridge University Press, Cambridge, 1 edition.

Lindzen, R. S. and Kuo, H. L. (1969). A reliable method for numerical integration of large class of ordinary and partial differential equations. *Mon. Wea. Rev.*, 97:732–734.

Madden, R. A. and Julian, P. R. (1971). Detection of a 40-50 Day Oscillation in the Zonal Wind in the Tropical Pacific. *Journal of Atmospheric Sciences*, 28:702–708.

Majda, A. (2003). *Introduction to PDEs and waves for the atmosphere and ocean*. Courant Institute of Mathematical Sciences, American Mathematical Society.

Majda, A. and Klein, R. (2003). Systematic multi-scale models for the tropisc. *J. Atmos. Sci.*, 60(2):393–408.

Morton, K. and Mayers, D. (1994). *Numerical solution of partial differential equations*. Cambridge University Press, Cambridge.

Neelin, J. D. and Zeng, N. (2000). A Quasi-Equilibrium Tropical Circulation Model–Formulation*. *Journal of Atmospheric Sciences*, 57:1741–1766.

Pedlosky, J. (1987). *Geophysical Fluid Dynamics*. Springer Verlag, New York, 2 edition.

Peixoto, J. and Oort, A. (1992). *Physics of Climate*. Springer Verlag, New York.

Petoukhov, V., Ganopolski, A., and Claussen, M. (2003). POTSDAM - a set of atmosphere statistical- dynamical models: theoretical background. Technical Report 81, Potsdam Institute of Climate Impact Research (PIK).

Plumb, R. A. and Hou, A. Y. (1992). The Response of a Zonally Symmetric Atmosphere to Subtropical Thermal Forcing: Threshold Behavior. *Journal of Atmospheric Sciences*, 49:1790–1799.

Polvani, L. and Sobel, A. (2002). The Hadley circulation and the weak temperature gradient approximation . *J. Atmos. Sci.*, 59:1744–1752.

Press, W., S.Teukolsky, W.Vetterling, and Flannery, B. (2002). *Numerical recipes in C++*. Cambridge University Press, Cambridge, 2 edition.

Riehl, H. (1979). *Climate and weather in the tropics*. Academic Press.

Roedel, W. (1994). *Physik unserer Umwelt: Die Atmosphäre.* Springer, Berlin.

Schneider, E. (1977). Axially symmetric steady-state models of the basic state for instability and climate studies. part ii nonlinear calculations. *J. Atmos. Sci.*, 34:280–296.

Schneider, E. and Lindzen, R. (1976). A discussion of the parametrization of momentum exchange by cumulus convection. *J. Geoph. Res.*, 81(18):3158–3160.

Schneider, E. and Lindzen, R. (1977). Axially symmetric steady-state models of the basic state for instability and climate studies. part i linearized calculations. *J. Atmos. Sci.*, 34:263–279.

Schneider, E. K. (1987). A Simplified Model of the Modified Hadley Circulation. *Journal of Atmospheric Sciences*, 44:3311–3328.

Sobel, A., Nilson, J., and Polvani, L. (2001). The weak temperature gradient approximation and balanced tropical moisture was. *J. Atmos. Sci.*, 58:3650–3665.

Wang, B. and Li, T. (1993). A simple atmosphere model of relevance to short-term climat variations. *J. Atmos. Sci.*, 50(2):260–284.

Wang, B. and Li, T. (1994). Convective Interaction with Boundary-Layer Dynamics in the Development of a Tropical Intraseasonal System. *Journal of Atmospheric Sciences*, 51:1386–1400.

Zeng, N., Neelin, J. D., and Chou, C. (2000). A Quasi-Equilibrium Tropical Circulation Model–Implementation and Simulation*. *Journal of Atmospheric Sciences*, 57:1767–1796.

PIK Report-Reference:

No. 1 3. Deutsche Klimatagung, Potsdam 11.-14. April 1994
Tagungsband der Vorträge und Poster (April 1994)

No. 2 Extremer Nordsommer '92
Meteorologische Ausprägung, Wirkungen auf naturnahe und vom Menschen beeinflußte Ökosysteme, gesellschaftliche Perzeption und situationsbezogene politisch-administrative bzw. individuelle Maßnahmen (Vol. 1 - Vol. 4)
H.-J. Schellnhuber, W. Enke, M. Flechsig (Mai 1994)

No. 3 Using Plant Functional Types in a Global Vegetation Model
W. Cramer (September 1994)

No. 4 Interannual variability of Central European climate parameters and their relation to the large-scale circulation
P. C. Werner (Oktober 1994)

No. 5 Coupling Global Models of Vegetation Structure and Ecosystem Processes - An Example from Arctic and Boreal Ecosystems
M. Plöchl, W. Cramer (Oktober 1994)

No. 6 The use of a European forest model in North America: A study of ecosystem response to climate gradients
H. Bugmann, A. Solomon (Mai 1995)

No. 7 A comparison of forest gap models: Model structure and behaviour
H. Bugmann, Y. Xiaodong, M. T. Sykes, Ph. Martin, M. Lindner, P. V. Desanker, S. G. Cumming (Mai 1995)

No. 8 Simulating forest dynamics in complex topography using gridded climatic data
H. Bugmann, A. Fischlin (Mai 1995)

No. 9 Application of two forest succession models at sites in Northeast Germany
P. Lasch, M. Lindner (Juni 1995)

No. 10 Application of a forest succession model to a continentality gradient through Central Europe
M. Lindner, P. Lasch, W. Cramer (Juni 1995)

No. 11 Possible Impacts of global warming on tundra and boreal forest ecosystems - Comparison of some biogeochemical models
M. Plöchl, W. Cramer (Juni 1995)

No. 12 Wirkung von Klimaveränderungen auf Waldökosysteme
P. Lasch, M. Lindner (August 1995)

No. 13 MOSES - Modellierung und Simulation ökologischer Systeme - Eine Sprachbeschreibung mit Anwendungsbeispielen
V. Wenzel, M. Kücken, M. Flechsig (Dezember 1995)

No. 14 TOYS - Materials to the Brandenburg biosphere model / GAIA
Part 1 - Simple models of the "Climate + Biosphere" system
Yu. Svirezhev (ed.), A. Block, W. v. Bloh, V. Brovkin, A. Ganopolski, V. Petoukhov, V. Razzhevaikin (Januar 1996)

No. 15 Änderung von Hochwassercharakteristiken im Zusammenhang mit Klimaänderungen - Stand der Forschung
A. Bronstert (April 1996)

No. 16 Entwicklung eines Instruments zur Unterstützung der klimapolitischen Entscheidungsfindung
M. Leimbach (Mai 1996)

No. 17 Hochwasser in Deutschland unter Aspekten globaler Veränderungen - Bericht über das DFG-Rundgespräch am 9. Oktober 1995 in Potsdam
A. Bronstert (ed.) (Juni 1996)

No. 18 Integrated modelling of hydrology and water quality in mesoscale watersheds
V. Krysanova, D.-I. Müller-Wohlfeil, A. Becker (Juli 1996)

No. 19 Identification of vulnerable subregions in the Elbe drainage basin under global change impact
V. Krysanova, D.-I. Müller-Wohlfeil, W. Cramer, A. Becker (Juli 1996)

No. 20 Simulation of soil moisture patterns using a topography-based model at different scales
D.-I. Müller-Wohlfeil, W. Lahmer, W. Cramer, V. Krysanova (Juli 1996)

No. 21 International relations and global climate change
D. Sprinz, U. Luterbacher (1st ed. July, 2n ed. December 1996)

No. 22 Modelling the possible impact of climate change on broad-scale vegetation structure - examples from Northern Europe
W. Cramer (August 1996)

No. 23 A methode to estimate the statistical security for cluster separation
F.-W. Gerstengarbe, P.C. Werner (Oktober 1996)

No. 24 Improving the behaviour of forest gap models along drought gradients
H. Bugmann, W. Cramer (Januar 1997)

No. 25 The development of climate scenarios
P.C. Werner, F.-W. Gerstengarbe (Januar 1997)

No. 26 On the Influence of Southern Hemisphere Winds on North Atlantic Deep Water Flow
S. Rahmstorf, M. H. England (Januar 1977)

No. 27 Integrated systems analysis at PIK: A brief epistemology
A. Bronstert, V. Brovkin, M. Krol, M. Lüdeke, G. Petschel-Held, Yu. Svirezhev, V. Wenzel (März 1997)

No. 28 Implementing carbon mitigation measures in the forestry sector - A review
M. Lindner (Mai 1997)

No. 29 Implementation of a Parallel Version of a Regional Climate Model
M. Kücken, U. Schättler (Oktober 1997)

No. 30 Comparing global models of terrestrial net primary productivity (NPP): Overview and key results
W. Cramer, D. W. Kicklighter, A. Bondeau, B. Moore III, G. Churkina, A. Ruimy, A. Schloss, participants of "Potsdam '95" (Oktober 1997)

No. 31 Comparing global models of terrestrial net primary productivity (NPP): Analysis of the seasonal behaviour of NPP, LAI, FPAR along climatic gradients across ecotones
A. Bondeau, J. Kaduk, D. W. Kicklighter, participants of "Potsdam '95" (Oktober 1997)

No. 32 Evaluation of the physiologically-based forest growth model FORSANA
R. Grote, M. Erhard, F. Suckow (November 1997)

No. 33 Modelling the Global Carbon Cycle for the Past and Future Evolution of the Earth System
S. Franck, K. Kossacki, Ch. Bounama (Dezember 1997)

No. 34 Simulation of the global bio-geophysical interactions during the Last Glacial Maximum
C. Kubatzki, M. Claussen (Januar 1998)

No. 35 CLIMBER-2: A climate system model of intermediate complexity. Part I: Model description and performance for present climate
V. Petoukhov, A. Ganopolski, V. Brovkin, M. Claussen, A. Eliseev, C. Kubatzki, S. Rahmstorf (Februar 1998)

No. 36 Geocybernetics: Controlling a rather complex dynamical system under uncertainty
H.-J. Schellnhuber, J. Kropp (Februar 1998)

No. 37 Untersuchung der Auswirkungen erhöhter atmosphärischer CO_2-Konzentrationen auf Weizenbestände des Free-Air Carbondioxid Enrichment (FACE) - Experimentes Maricopa (USA)
T. Kartschall, S. Grossman, P. Michaelis, F. Wechsung, J. Gräfe, K. Waloszczyk, G. Wechsung, E. Blum, M. Blum (Februar 1998)

No. 38 Die Berücksichtigung natürlicher Störungen in der Vegetationsdynamik verschiedener Klimagebiete
K. Thonicke (Februar 1998)

No. 39 Decadal Variability of the Thermohaline Ocean Circulation
S. Rahmstorf (März 1998)

No. 40 SANA-Project results and PIK contributions
K. Bellmann, M. Erhard, M. Flechsig, R. Grote, F. Suckow (März 1998)

No. 41 Umwelt und Sicherheit: Die Rolle von Umweltschwellenwerten in der empirisch-quantitativen Modellierung
D. F. Sprinz (März 1998)

No. 42 Reversing Course: Germany's Response to the Challenge of Transboundary Air Pollution
D. F. Sprinz, A. Wahl (März 1998)

No. 43 Modellierung des Wasser- und Stofftransportes in großen Einzugsgebieten. Zusammenstellung der Beiträge des Workshops am 15. Dezember 1997 in Potsdam
A. Bronstert, V. Krysanova, A. Schröder, A. Becker, H.-R. Bork (eds.) (April 1998)

No. 44 Capabilities and Limitations of Physically Based Hydrological Modelling on the Hillslope Scale
A. Bronstert (April 1998)

No. 45 Sensitivity Analysis of a Forest Gap Model Concerning Current and Future Climate Variability
P. Lasch, F. Suckow, G. Bürger, M. Lindner (Juli 1998)

No. 46 Wirkung von Klimaveränderungen in mitteleuropäischen Wirtschaftswäldern
M. Lindner (Juli 1998)

No. 47 SPRINT-S: A Parallelization Tool for Experiments with Simulation Models
M. Flechsig (Juli 1998)

No. 48 The Odra/Oder Flood in Summer 1997: Proceedings of the European Expert Meeting in Potsdam, 18 May 1998
A. Bronstert, A. Ghazi, J. Hladny, Z. Kundzewicz, L. Menzel (eds.) (September 1998)

No. 49 Struktur, Aufbau und statistische Programmbibliothek der meteorologischen Datenbank am Potsdam-Institut für Klimafolgenforschung
H. Österle, J. Glauer, M. Denhard (Januar 1999)

No. 50 The complete non-hierarchical cluster analysis
F.-W. Gerstengarbe, P. C. Werner (Januar 1999)

No. 51 Struktur der Amplitudengleichung des Klimas
A. Hauschild (April 1999)

No. 52 Measuring the Effectiveness of International Environmental Regimes
C. Helm, D. F. Sprinz (Mai 1999)

No. 53 Untersuchung der Auswirkungen erhöhter atmosphärischer CO_2-Konzentrationen innerhalb des Free-Air Carbon Dioxide Enrichment-Experimentes: Ableitung allgemeiner Modellösungen
T. Kartschall, J. Gräfe, P. Michaelis, K. Waloszczyk, S. Grossman-Clarke (Juni 1999)

No. 54 Flächenhafte Modellierung der Evapotranspiration mit TRAIN
L. Menzel (August 1999)

No. 55 Dry atmosphere asymptotics
N. Botta, R. Klein, A. Almgren (September 1999)

No. 56 Wachstum von Kiefern-Ökosystemen in Abhängigkeit von Klima und Stoffeintrag - Eine regionale Fallstudie auf Landschaftsebene
M. Erhard (Dezember 1999)

No. 57 Response of a River Catchment to Climatic Change: Application of Expanded Downscaling to Northern Germany
D.-I. Müller-Wohlfeil, G. Bürger, W. Lahmer (Januar 2000)

No. 58 Der "Index of Sustainable Economic Welfare" und die Neuen Bundesländer in der Übergangsphase
V. Wenzel, N. Herrmann (Februar 2000)

No. 59 Weather Impacts on Natural, Social and Economic Systems (WISE, ENV4-CT97-0448) German report
M. Flechsig, K. Gerlinger, N. Herrmann, R. J. T. Klein, M. Schneider, H. Sterr, H.-J. Schellnhuber (Mai 2000)

No. 60 The Need for De-Aliasing in a Chebyshev Pseudo-Spectral Method
M. Uhlmann (Juni 2000)

No. 61 National and Regional Climate Change Impact Assessments in the Forestry Sector - Workshop Summary and Abstracts of Oral and Poster Presentations
M. Lindner (ed.) (Juli 2000)

No. 62 Bewertung ausgewählter Waldfunktionen unter Klimaänderung in Brandenburg
A. Wenzel (August 2000)

No. 63 Eine Methode zur Validierung von Klimamodellen für die Klimawirkungsforschung hinsichtlich der Wiedergabe extremer Ereignisse
U. Böhm (September 2000)

No. 64 Die Wirkung von erhöhten atmosphärischen CO_2-Konzentrationen auf die Transpiration eines Weizenbestandes unter Berücksichtigung von Wasser- und Stickstofflimitierung
S. Grossman-Clarke (September 2000)

No. 65 European Conference on Advances in Flood Research, Proceedings, (Vol. 1 - Vol. 2)
A. Bronstert, Ch. Bismuth, L. Menzel (eds.) (November 2000)

No. 66 The Rising Tide of Green Unilateralism in World Trade Law - Options for Reconciling the Emerging North-South Conflict
F. Biermann (Dezember 2000)

No. 67 Coupling Distributed Fortran Applications Using C++ Wrappers and the CORBA Sequence Type
T. Slawig (Dezember 2000)

No. 68 A Parallel Algorithm for the Discrete Orthogonal Wavelet Transform
M. Uhlmann (Dezember 2000)

No. 69 SWIM (Soil and Water Integrated Model), User Manual
V. Krysanova, F. Wechsung, J. Arnold, R. Srinivasan, J. Williams (Dezember 2000)

No. 70 Stakeholder Successes in Global Environmental Management, Report of Workshop, Potsdam, 8 December 2000
M. Welp (ed.) (April 2001)

No. 71 GIS-gestützte Analyse globaler Muster anthropogener Waldschädigung - Eine sektorale Anwendung des Syndromkonzepts
M. Cassel-Gintz (Juni 2001)

No. 72 Wavelets Based on Legendre Polynomials
J. Fröhlich, M. Uhlmann (Juli 2001)

No. 73 Der Einfluß der Landnutzung auf Verdunstung und Grundwasserneubildung - Modellierungen und Folgerungen für das Einzugsgebiet des Glan
D. Reichert (Juli 2001)

No. 74 Weltumweltpolitik - Global Change als Herausforderung für die deutsche Politikwissenschaft
F. Biermann, K. Dingwerth (Dezember 2001)

No. 75 Angewandte Statistik - PIK-Weiterbildungsseminar 2000/2001
F.-W. Gerstengarbe (Hrsg.) (März 2002)

No. 76 Zur Klimatologie der Station Jena
B. Orlowsky (September 2002)

No. 77 Large-Scale Hydrological Modelling in the Semi-Arid North-East of Brazil
A. Güntner (September 2002)

No. 78 Phenology in Germany in the 20th Century: Methods, Analyses and Models
J. Schaber (November 2002)

No. 79 Modelling of Global Vegetation Diversity Pattern
I. Venevskaia, S. Venevsky (Dezember 2002)

No. 80 Proceedings of the 2001 Berlin Conference on the Human Dimensions of Global Environmental Change “Global Environmental Change and the Nation State”
F. Biermann, R. Brohm, K. Dingwerth (eds.) (Dezember 2002)

No. 81 POTSDAM - A Set of Atmosphere Statistical-Dynamical Models: Theoretical Background
V. Petoukhov, A. Ganopolski, M. Claussen (März 2003)

No. 82 Simulation der Siedlungsflächenentwicklung als Teil des Globalen Wandels und ihr Einfluß auf den Wasserhaushalt im Großraum Berlin
B. Ströbl, V. Wenzel, B. Pfützner (April 2003)

No. 83 Studie zur klimatischen Entwicklung im Land Brandenburg bis 2055 und deren Auswirkungen auf den Wasserhaushalt, die Forst- und Landwirtschaft sowie die Ableitung erster Perspektiven
F.-W. Gerstengarbe, F. Badeck, F. Hattermann, V. Krysanova, W. Lahmer, P. Lasch, M. Stock, F. Suckow, F. Wechsung, P. C. Werner (Juni 2003)

No. 84 Well Balanced Finite Volume Methods for Nearly Hydrostatic Flows
N. Botta, R. Klein, S. Langenberg, S. Lützenkirchen (August 2003)

No. 85 Orts- und zeitdiskrete Ermittlung der Sickerwassermenge im Land Brandenburg auf der Basis flächendeckender Wasserhaushaltsberechnungen
W. Lahmer, B. Pfützner (September 2003)

No. 86 A Note on Domains of Discourse - Logical Know-How for Integrated Environmental Modelling, Version of October 15, 2003
C. C. Jaeger (Oktober 2003)

No. 87 Hochwasserrisiko im mittleren Neckarraum - Charakterisierung unter Berücksichtigung regionaler Klimaszenarien sowie dessen Wahrnehmung durch befragte Anwohner
M. Wolff (Dezember 2003)

No. 88 Abflußentwicklung in Teileinzugsgebieten des Rheins - Simulationen für den Ist-Zustand und für Klimaszenarien
D. Schwandt (April 2004)

No. 89 Regionale Integrierte Modellierung der Auswirkungen von Klimaänderungen am Beispiel des semi-ariden Nordostens von Brasilien
A. Jaeger (April 2004)

No. 90 Lebensstile und globaler Energieverbrauch - Analyse und Strategieansätze zu einer nachhaltigen Energiestruktur
F. Reusswig, K. Gerlinger, O. Edenhofer (Juli 2004)

No. 91 Conceptual Frameworks of Adaptation to Climate Change and their Applicability to Human Health
H.-M. Füssel, R. J. T. Klein (August 2004)

No. 92 Double Impact - The Climate Blockbuster ’The Day After Tomorrow’ and its Impact on the German Cinema Public
F. Reusswig, J. Schwarzkopf, P. Polenz (Oktober 2004)

No. 93 How Much Warming are we Committed to and How Much Can be Avoided?
B. Hare, M. Meinshausen (Oktober 2004)

No. 94 Urbanised Territories as a Specific Component of the Global Carbon Cycle
A. Svirejeva-Hopkins, H.-J. Schellnhuber (Januar 2005)

No. 95 GLOWA-Elbe I - Integrierte Analyse der Auswirkungen des globalen Wandels auf Wasser, Umwelt und Gesellschaft im Elbegebiet
F. Wechsung, A. Becker, P. Gräfe (Hrsg.) (April 2005)

No. 96 The Time Scales of the Climate-Economy Feedback and the Climatic Cost of Growth
S. Hallegatte (April 2005)

No. 97 A New Projection Method for the Zero Froude Number Shallow Water Equations
S. Vater (Juni 2005)

No. 98 Table of EMICs - Earth System Models of Intermediate Complexity
M. Claussen (ed.) (Juli 2005)

No. 99 KLARA - Klimawandel - Auswirkungen, Risiken, Anpassung
M. Stock (Hrsg.) (Juli 2005)

No. 100 Katalog der Großwetterlagen Europas (1881-2004) nach Paul Hess und Helmut Brezowsky 6., verbesserte und ergänzte Auflage
F.-W. Gerstengarbe, P. C. Werner (September 2005)

No. 101 An Asymptotic, Nonlinear Model for Anisotropic, Large-Scale Flows in the Tropics
S. Dolaptchiev (September 2005)